ISSN: 2164-3024 Volume 13, Number 2, June 2023

Scientific Research Publishing

Open Journal of Radiology

Journal Editorial Board

ISSN Print: 2164-3024 ISSN Online: 2164-3032

https://www.scirp.org/journal/ojrad

Open Journal of Radiology, 2023, 13, 87-123
https://www.scirp.org/journal/ojrad
ISSN Online: 2164-3032
ISSN Print: 2164-3024

Table of Contents

Volume 13 Number 2 June 2023

Open Journal of Radiology (OJRad)
Journal Information

SUBSCRIPTIONS

The *Open Journal of Radiology* (Online at Scientific Research Publishing, https://www.scirp.org/) is published quarterly by Scientific Research Publishing, Inc., USA.

Subscription rates:
Print: $79 per issue.
To subscribe, please contact Journals Subscriptions Department, E-mail: sub@scirp.org

SERVICES

Advertisements
Advertisement Sales Department, E-mail: service@scirp.org

Reprints (minimum quantity 100 copies)
Reprints Co-ordinator, Scientific Research Publishing, Inc., USA.
E-mail: sub@scirp.org

COPYRIGHT

PRODUCTION INFORMATION

For manuscripts that have been accepted for publication, please contact:
E-mail: ojrad@scirp.org

Open Journal of Radiology, 2023, 13, 87-93
https://www.scirp.org/journal/ojrad
ISSN Online: 2164-3032
ISSN Print: 2164-3024

Evaluation of Brain CT Images of Eclamptics in Portharcourt Nigeria

Job Gogo Otokwala[1], Emmanuel Chukuemeka Agi[2*]

[1]Intensive Care Unit, Department of Anaesthesiology, University of Port, Harcourt, Nigeria
[2]Department of Radiology, University of Port, Harcourt, Nigeria
Email: *achukuemeka@hotmail.com

How to cite this paper: Otokwala, J.G and Agi, E.C. (2023) Evaluation of Brain CT Images of Eclamptics in Portharcourt Nigeria. *Open Journal of Radiology*, **13**, 87-93.
https://doi.org/10.4236/ojrad.2023.132009

Received: March 22, 2023
Accepted: May 16, 2023
Published: May 19, 2023

Abstract

Eclampsia is a common complication of hypertensive disorders of pregnancy and in the puerperium with the attendant risk to both the mother and baby. Although it is a multi-systemic disorder, its manifestation that affects the brain and resulting in altered sensorium demands brain imaging to define the possible brain lesions and the implications for critical care management and outcome. We evaluated the CT brain lesions in the patients with eclampsia who were admitted in the intensive care unit, University of Port Harcourt, Port Harcourt Nigeria. Objective: To analyse the CT brain images of eclamptic parturients and the outcome following their admission in the intensive care unit. Methods: We undertook this observational study after obtaining ethical exemption from the University of Portharcourt Teaching Hospital ethical review board, and commenced the review between March 2021 to February 2023. We included all parturients that were admitted into the intensive care unit of the University of Portharcourt Teaching Hospital, a nine-bedded open intensive care unit with the clinical diagnosis of eclampsia. Every admitted parturient was required to obtain a brain computed tomography (CT) by local protocol. The brain CT images were retrieved for review from the parturients' relatives, radiology department and the ICU. Parturients included were aged ≥ 18 years. The radiological reports of these brain images which were also reviewed by a neurosurgeon in case of any need for secondary opinion were subjected to statistical analysis. Result: Thirty-one parturients were admitted with eclampsia with a mean age of 30 years ± 5.29. Sixteen (16) parturients died representing 52%. Only twenty-four (24) CT brain images were retrieved for review (77%). The following brain lesions were identified from the brain CT and they comprised the following: intracerebral haemorrhage, including extensions into the ventricles 7 (29.17%), cerebral oedema 12 (50%), subdural hematoma 1 (4.17%) and normal imaging 4 (16.66%). The subdural haematoma was promptly evacuated with a good outcome. Conclusion: Neuro imaging comprising computed tomography and magnetic resonance imaging of the brain are basic ancillary investigations for patients with eclampsia presenting with neurologic deficits and low GCS. Early presentation and access to brain CT could influence outcome as it was demonstrated in the prompt intervention in the patient with subdural haematoma which was evacuated with a satisfactory outcome.

Keywords

Evaluation, Eclamptics, Brain CT, Intensive Care Unit, Portharcourt

1. Introduction

In Nigeria, eclampsia, which is a complication of the hypertensive disorders of pregnancy is a common phenomenon and a causation of maternal mortality and morbidity. The prevalence in Nigeria varies between 1 in 12 to 1 in 1,700 deliveries [1] [2]. This is associated with high mortality, which was reported to be in excess of 31.9% - 46.4% [3] [4]. It was observed that about 0.8% of women with hypertensive disorders of pregnancy ended up with eclampsia [5]. Although the cause of eclamptic seizure is obscure, it is reported that it involves the disruption of blood-brain barrier with the influx of ions, fluids, plasma proteins and some vasoactive factors into the brain parenchyma, and these blood particles have the tendency to trigger microglial activation [6] [7] [8] which have been found to be a seizure threshold lowering agent [9]. Several theories have been espoused to define the possible cause of brain pathologies in eclamptics and these include but not limited to the following: the loss of cerebral autoregulation with blood brain barrier disruption [10] [11] [12], a possible shift in the autoregulation curve in pregnancy to a much lower blood pressure [13] [14] to vascular dysfunction with the activation of superoxide in the endothelial cells.

Autopsy findings of massive cerebral oedema, white matter haemorrhage and necrosis all support the influence of autoregulation dysfunction with the loss of blood brain barrier as a common pathway to the onset of seizures and altered sensorium seen in eclamptics [15].

Following from above, does neuroimaging have a role in the management of eclampsia? It is observed that parturients with focal neurological deficits, recurrent seizures especially those occurring in the second trimester, or prolonged coma require neuroimaging. The presence of intracranial abnormalities may require surgical intervention, in the case of haemorrhage or pharmacological treatments. The essence of this paper therefore was to evaluate the type and proportion of brain lesions seen in eclamptic women that presented in the intensive care unit at the University of Port Harcourt Teaching Hospital Nigeria and the observed outcome.

2. Methodology

We undertook this non randomised retrospective observational review of the brain computed tomography (CT) images of all eclamptic parturients on admission at the intensive care unit (ICU) of the University of Port Harcourt Teaching Hospital Port Harcourt Nigeria, during the study period March 2021-February 2023, a nine hundred and twenty bedded tertiary teaching hospital with a nine bedded ICU which sub serves all medical and surgical units. We obtained ethical exemption from the hospital's research and ethics review board. Every admitted parturient was required to obtain a brain computed tomography (CT) by local protocol. The brain CT images were retrieved for review from the parturients' relatives, radiology department and the ICU. The radiological reports of these brain images were also reviewed by the in house neurosurgeon in case of any need for secondary opinion. Sample size for retrospective study for 13months was calculated based on the available sample size (N = 31).

Inclusion criteria included: Adults ≥ 18 years with clinical diagnosis of eclampsia presenting with neurological deficits during pregnancy and the puerperium and must be admitted into the intensive care unit (ICU) for more than twenty-four hours. Parturients must have retrieved brain CT images and all images must be read by a consultant radiologist. All brain CT images that could not be retrieved were excluded from the study. Parturients with known intracranial pathologies such as tumours and seizure disorder were excluded. Patients with mental health problems were also excluded.

The descriptive data of the parturients were obtained from the ICU register as well as the radiological unit register. These comprise: age, co-morbidity, brain CT lesion and outcome. Statistical analysis was performed using Jamovi statistical software version1.2 (https://www.jamovi.org) accessed 01/03/2023.

3. Results

A total of 31 parturients were admitted with a clinical diagnosis of eclampsia in 13months. Access to brain CT was available for review in only twenty-four patients (77%) and these were analysed and presented in this study. The mean age of parturients was 30.6 ± 5.9 years. Sixteen parturients died (51.6%). Retrieved CT images were 24 (77.4%) while 7 (22.6%) images could not be retrieved. CT findings depicted the following: Subdural haematoma 1 (4.17%), Intracerebral haemorrhage 7 (29.17%), Cerebral oedema 12 (50.0%), normal imaging 4 (16.66%). All the parturients were admitted postpartum and mostly from the Unbooked labour ward. The affected parts of the brain included the right parieto-occipital lobe, effacement of the cerebral sulci and gyri with associated compression of the anterior and posterior horns due to cerebral oedema. Other parts of the brain involved included: the left occipital lobe white matter, right occipital lobe infarct, left sided acute intracerebral and occipital lobe haemorrhage and Left sided subdural haematoma.

4. Discussion

The usefulness of neuroimaging especially the brain CT in defining the management and prognosis of eclamptics has been reported in the literature [16] and in this study, the relevance of neuroimaging as a guide became much more valuable in deciding possible interventions for the critically-ill parturients with eclampsia in Nigeria.

One major organ that is grossly affected by eclampsia is the brain. Autopsy findings in eclamptics had revealed the presence of massive cerebral oedema, white matter haemorrhages and necrosis [6]. Vasogenicoedema arising from endothelial damage has been implicated along the distribution of the posterior cerebral arteries [17] affecting the parieto-occipital lobes. In clinical observations, the brain CT and MRI are commonly used in patients with signs of focal neurological deficits, seizures and altered sensorium, with the CT having the superiority in diagnosing haemorrhages and cerebral oedema [18]. Majority of the patients studied in this report were in their 30s, this was similar to other observations [16] [17]. The high mortality rate is also consistent with other reports [19] [20] and affected mostly patients in Unbooked labour wards. These subsets of patients are usually poor and could barely afford brain CT, often present late to critical care and this could also account for the delay to access brain CT. The time lag and late presentation could have contributed to the high mortality. One case of subdural haematoma as shown in the result (**Figure 1**) was identified in this study, in a patient that could have been passively managed as routine eclamptic but surgical evacuation was promptly done in this case with rapid recovery of neurological deficits. The other CT findings included: intracerebral haemorrhage (**Figure 2** and **Figure 4**) affecting the parietal lobe similar to the report of MC Kinney *et al.* [21]. Cerebral oedema (**Figure 3**) was the commonest finding in this study, representing about 50% of the CT findings. This was similar to the reports of Richard *et al.* [22] and others [23]. Is there regional variation in the brain lesions in eclampsia, this may be a push for further evaluation. While cerebral infarct was commoner in a Canadian series [24], the French, reported more of cerebral oedema [25], and in our study, a preponderance of cerebral oedema (**Figure 3**) and intracerebral bleed (**Figure 2** and **Figure 4**). It was

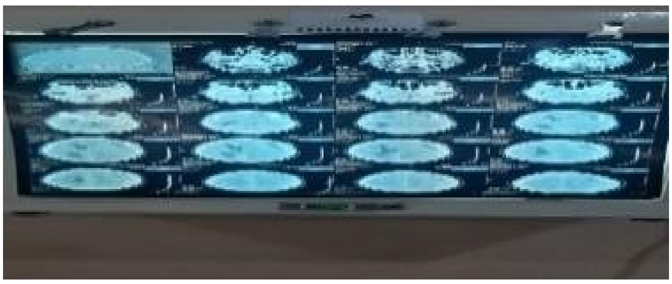

Figure 1. Showing left sidedsubacute subdural haematoma with effacement of the ipsilateral lateral ventricle as well as deviation (herniation) of the falxcerebri. There was elevated intracranial pressure and falcine herniation and displacement.

Figure 2. Right sided acute intraventricular and intracerebral (parieto-occipital lobe) haemorrhage.

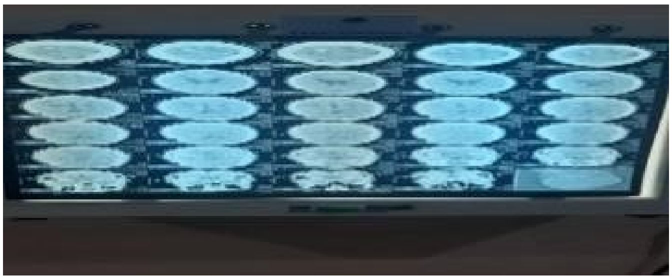

Figure 3. Effacement of the cerebral sulci and gyri with compression of the ventricles. Impression: cerebral.

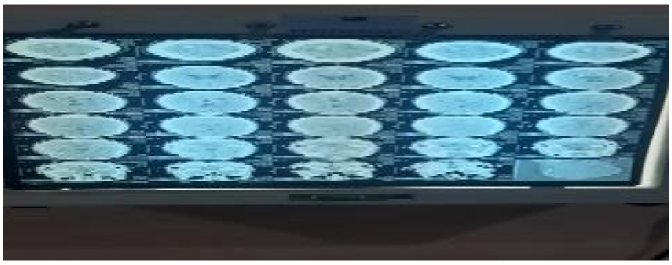

Figure 4. There is hyper dense area (acute bleed) in the left occipital lobe white matter. An ill-defined hypo dense area is seen in the right occipital lobe, indicating left side acute intracerebral (occipital lobe) haemorrhage. Right sided occipital lobe infarct.

also observed in this study that there were some cases with no obvious abnormality as detected on brain CT, this could be supported by the observation by Hamandou *et al.* [25] of cerebral oedema being seen in eclamptics with apparently normal brain CT but on MRI. Cost to access these investigations in resource limited settings reflects the apparently low yield of neuroimaging in an eclampsia rich environment. The care required for all eclampsia patients remain the same with strong neuro protective support and other measures to optimise functional reserves and drive improved outcome.

5. Conclusions

It is routine to do brain CT for all eclamptics presenting with signs of neurological deficit.

Prompt intervention with neurocritical care bundles, such as early airway protection and mechanical ventilation and all ancillary neuro protective measures will obviate further deteriorations which are a major cause of maternal morbidity and mortality.

Conflicts of Interest

The authors declare no conflicts of interest regarding the publication of this paper.

References

[1] World Health Organization International Collaborative Study of Hypertensive Disorders of Pregnancy (1998) Geographic Variations in the Incidence of Hypertension in Pregnancy. *American Journal of Obstetrics and Gynecology*, **151**, 80-83.

[2] Knight, M. (2007) Eclampsia in the United Kingdom 2005. *BJOG: An International Journal of Obstetrics & Gynaecology*, **114**, 1072-1078. https://doi.org/10.1111/j.1471-0528.2007.01423.x

[3] Lee, W., O'Connell, C.M. and Baskett, T.F. (2004) Maternal and Perinatal Outcomes of Eclampsia: Nosa Scotia, 1981-2000. *Journal of Obstetrics and Gynaecology Canada*, **26**, 119-123. https://doi.org/10.1016/S1701-2163(16)30487-X

[4] Begum, M.R., Begum, A., Quadir, E., Akhter, S. and Shamsuddin, L. (2004) Eclampsia: Still a Problem in Bangladesh. *Medscape General Medicine*, **6**, Article 52.

[5] Altman, D., Carroli, G., Duley, L., *et al.* (2002) Do Women with Preeclampsia, and Their Babies, Benefit from Magnesium Sulphate? The Magpie Trial: A Randomized Placebo-Controlled Trial. *The Lancet*, **359**, 1877-1890. https://doi.org/10.1016/S0140-6736(02)08778-0

[6] Marchi, N., Tierney, W., Alexopoulos, A.V., Puvenna, V., Granata, T. and Janigro, D. (2011) The Aetiological Role of Blood Brain Barrier Dysfunction in Seizure Disorders. *Cardiovascular Psychiatry and Neurology*, **2011**, Article ID: 482415. https://doi.org/10.1155/2011/482415

[7] Johnson, A.C., Tremble, S.M., Chan, S.L., *et al.* (2014) Magnesium Sulfate Treatment Reverses Seizure Susceptibility and Decreases Neuroinflammation in a Rat Model of Severe Preeclampsia. *PLOS ONE*, **9**, e113670. https://doi.org/10.1371/journal.pone.0113670

[8] Oby, E. and Janigro, D. (2022) The Blood-Brain Barrier and Epilepsy. *Epilepsia*, **47**, 1761-1774. https://doi.org/10.1111/j.1528-1167.2006.00817.x

[9] Michal, F.B. and Baha, M.S. (2022) Eclampsia in the 21st Century. *American Journal of Obstetrics and Gynecology*, **226**, S1237-S1253. https://doi.org/10.1016/j.ajog.2020.09.037

[10] Jones-Muhammad, M. and Warrington, J.P. (2019) Cerebral Blood Flow Regulation in Pregnancy, Hypertension and Hypertensive Disorders of Pregnancy. *Brain Sciences*, **2019**, Article 224. https://doi.org/10.3390/brainsci9090224

[11] Cipolla, M.J., Bishop, N. and Chan, S.L. (2012) Effect of Pregnancy on Autoregulation of Cerebral Blood Flow in Anterior versus Posterior Cerebrum. *Hypertension*, **60**, 705-711. https://doi.org/10.1161/HYPERTENSIONAHA.112.198952

[12] Friedman, A., Kaufer, D. and Heinemann, U. (2009) Blood-Brain Barrier Breakdown Inducing Astrocytic Transformation: Novel Targets for the Prevention of Epilepsy. *Epilepsy Research*, **85**, 142-149. https://doi.org/10.1016/j.eplepsyres.2009.03.005

[13] Chapman, A.C., Cipolla, M.J. and Chan, S.L. (2013) Effect of Pregnancy and Nitric

oxide on Myogenic Vasodilation of Posterior Cerebral Arteries and the Lower Limit of Cerebral Blood Flow Autoregulation. *Reproductive Sciences*, **20**, 1046-1054. https://doi.org/10.1177/1933719112473661

[14] Cipolla, M.J., Vitullo, L. and McKinnon, J. (2004) Cerebral Artery Reactivity Changes during Pregnancy and the Postpartum Period: A Role in Eclampsia? *American Journal of Physiology-Heart and Circulatory Physiology*, **286**, H2127-H2132. https://doi.org/10.1152/ajpheart.01154.2003

[15] Hecht, J.L., Ordi, J., Carrilho, C., *et al.* (2017) The Pathology of Eclampsia: An Autopsy Series. *Hypertension in Pregnancy*, **36**, 259-268. https://doi.org/10.1080/10641955.2017.1329430

[16] Madhavi, K.N., Guguloth, K., Sivaranjani, B.S.V. and Sreevalli, M. (2023) Computed Tomography Brain Scan Findings in Eclampsia. *International Journal of Reproduction, Contraception, Obstetrics and Gynecology*, **12**, 94-97. https://doi.org/10.18203/2320-1770.ijrcog20223257

[17] Royburt, M., Seidman, D.S., Serr, D.M. and Mashiah, S. (1991) Neurologic Involvement in Hypertensive Disease of Pregnancy. *Obstetrical & Gynecological Survey*, **46**, 656-664. https://doi.org/10.1097/00006254-199110000-00002

[18] Zhu, X.W. (1993) Cerebral Lesions in the Severe Pregnancy Induced Hypertension: 61 Cases of X-Ray Computed Tomography of the Brain. *Chinese Journal of Obstetrics and Gynecology*, **28**, 275-277.

[19] Rabiu, K.A., Adewunmi, A.A., Ottun, T.A., *et al.* (2018) Risk Factors for Maternal Mortality Associated with Eclampsia Presenting at a Nigerian Tertiary Hospital. *International Journal of Women's Health*, **10**, 715-721. https://doi.org/10.2147/IJWH.S178729

[20] Nwobodo, E.I. and Ahmed, Y. (2011) Maternal Mortality Associated with Eclampsia in Sokoto Nigeria. *Orient Journal of Medicine*, **23**, 1-4.

[21] McKinney, A.M., Short, J., Jruwit, C.L., *et al.* (2007) Posterior Reversible Encephalopathy Syndrome: Incidence of Atypical Regions of Involvement and Imaging Findings. *American Journal of Roentgenology*, **189**, 904-912. https://doi.org/10.2214/AJR.07.2024

[22] Richards, A., Graham, D. and Bullock, R. (1988) Clinicopathological Study of Neurological Complications Due to Hypertensive Disorders of Pregnancy. *Journal of Neurology, Neurosurgery, and Psychiatry*, **51**, 416-421. https://doi.org/10.1136/jnnp.51.3.416

[23] Brouh, Y., Konan, K.J. and Ouattara, A. (2016) Brain Lesions in Eclamptics: A Series of 39 Cases Admitted in an Intensive Care Unit. *Indian Journal of Critical Care Medicine*, **20**, 178-181. https://doi.org/10.4103/0972-5229.178183

[24] Jaigobin, C. and Silver, F.L. (2000) Stroke and Pregnancy. *Stroke*, **31**, 2948-2951. https://doi.org/10.1161/01.STR.31.12.2948

[25] Hamandou, M., Madani, N., Labibe, S., Messouak, O., *et al.* (2006) Neuroimaging Findings in Eclamptic Patients Still Symptomatic after 24 Hours: A Descriptive Study about 19 Cases. *Annales Françaises d'Anesthésie et de Réanimation*, **25**, 577-583. https://doi.org/10.1016/j.annfar.2006.02.022

Open Journal of Radiology, 2023, 13, 94-100
https://www.scirp.org/journal/ojrad
ISSN Online: 2164-3032
ISSN Print: 2164-3024

Interest of Computed Tomography in the Diagnosis of Intestinal Obstruction Due to an Internal Hernia of Unusual Location: The Falciform Ligament

Diallo Moustapha*, Diack Aminata, Ndaw Mame Diarra Bousso, Amar Ndeye Isseu, Diop Massamba, Diouf Cheikh Tidiane, Fall Amath, Ndiaye Abdou Rahmane, Soko Thierno Omar, Mbengue Ababacar

Department of Medical Imaging, Dakar Principal Hospital, Dakar, Senegal
Email: *daddykr@hotmail.fr

How to cite this paper: Moustapha, D., Aminata, D., Bousso, N.M.D., Isseu, A.N., Massamba, D., Tidiane, D.C., Amath, F., Rahmane, N.A., Omar, S.T. and Ababacar, M. (2023) Interest of Computed Tomography in the Diagnosis of Intestinal Obstruction Due to an Internal Hernia of Unusual Location: The Falciform Ligament. *Open Journal of Radiology*, **13**, 94-100.
https://doi.org/10.4236/ojrad.2023.132010

Received: April 25, 2023
Accepted: June 16, 2023
Published: June 19, 2023

Abstract

Pathological implications of the falciform ligament are rare and internal hernias are exceptional. The origin of the falciform ligament defect can be congenital or inflammatory (a satellite of acute cholecystitis) or even post-surgical. The internal hernias of the falciform ligament are most often revealed by an acute intestinal obstruction syndrome with an ischemic component. The scanner provides the benchmarking examination allowing us to conduct a positive diagnosis and see also the inherent complications, which drives us to take the appropriate and fast surgical procedures. It is an entity that must be known.

Keywords

Internal Hernia, Falciform Ligament, Scanner

1. Introduction

Internal hernias are protrusions of hollow abdominal viscera in an intraperitoneal orifice but which remains inside the abdominal cavity [1] [2]. They can be revealed through an acute picture of intestinal obstruction, most often with ischemic component by strangulation. The hernia with the falciform ligament is exceptional and often diagnosed intraoperatively [3] [4]. An emergency abdominal CT scan is the benchmarking examination [5]. It can help in preoperative diagnosis and guide surgical procedures. Thus, we report a case of internal hernia of the falciform ligament revealed on an abdominal CT scan, the purpose of which is to show the interest of CT in the diagnosis and the inherent complications of this pathology.

2. Observation

We report the case of a 78-year-old patient with no particular history who was admitted to the emergency room for abdominal pain with vomiting and without fever, lasting for a few hours. There was no stopping of materials and gases.

On examination, he presented a tusk in the epigastric region with a cry from the umbilicus. The biological examinations did not find any hydro-electrolyte disorder and the blood count was normal.

An abdominal and pelvic CT scan was performed urgently in front of the peritoneal irritation syndrome with helical acquisition in thin sections without and with injection of contrast product in the portal phase, covering the abdominal and pelvic region. There was only a protrusion of dilated small loops between the abdominal wall and the liver, accompanied by peritoneal fat, with a transitional zone in the shape of a bird's beak (**Figure 1** and **Figure 2**). A mechanical occlusion on internal hernia of the falciform ligament was then mentioned. We also noted pain in the small loops along with a lack of parietal enhancement associated with infiltration of peritoneal fat.

The surgical intervention had objectified a hernia of the falciform ligament through a large defect and necrotic loops (**Figure 3** and **Figure 4**). It had been performed during a median sub-umbilical laparotomy, a disinsertion with collapse of the falciform ligament, an ileal resection with terminal ileo-ileal anastomosis.

The postoperative course was simple. Histological examination revealed hemorrhagic necrosis of the intestinal wall without signs of malignancy.

3. Comments

The falciform ligament is a remnant of the ventral midgut. It is stretched sagittally

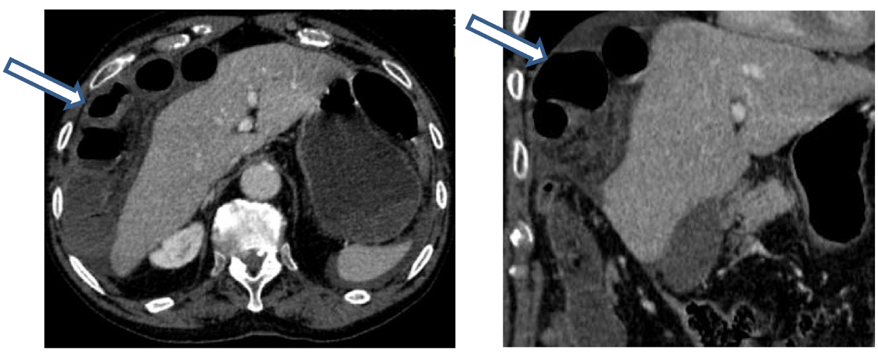

(a) (b)

Figure 1. Axial (a) and coronal (b) section of an abdominal CT scan with injection of contrast product in the portal phase: interposition of dilated small loops between the liver and the abdominal wall, accompanied by peritoneal fat (arrow).

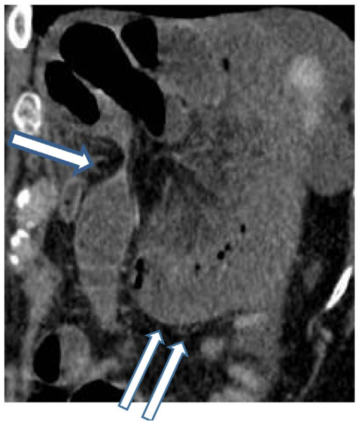

Figure 2. Sagital reconstruction of an abdominal CT scan with injection of contrast product: Transitional level reflecting the area of stricture (single arrow). Infiltration of peritoneal fat and lack of enhancement of the wall of the dilated small bowel loops (double arrow) suggesting ischemia.

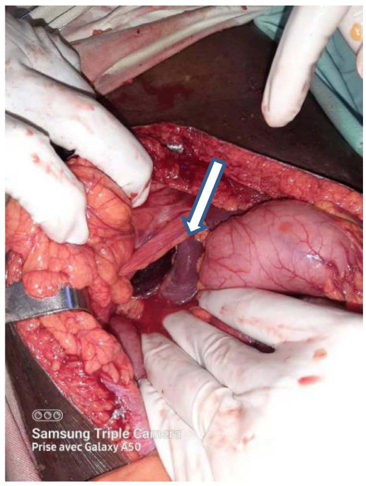

Figure 3. Intraoperative view showing a large falciform ligament defect (arrow) containing necrotic loops.

Figure 4. Intraoperative view after extrication showing viable loops (double arrow) and necrotic loops (single arrow).

from the superior surface of the liver to the inferior surface of the diaphragm and to the posterior surface of the abdominal wall. The two sheets which constitute it and which follow the upper sheet of the coronary ligament are formed by the reflection of the hepatic visceral peritoneum on the diaphragmatic peritoneum. It contains the round ligament, the para-umbilical veins and a variable degree of fat [6] [7].

Pathological implications of the falciform ligament are rare. Apart from hernias, gangrene, most often related to acute necrotizing pancreatitis, benign or non-benign tumors (lipomas and myxoid sarcomas in particular) and torsion of fatty fringes have been described [8] [9].

The internal abdominal hernias fall into two categories: the hernias developed in a normal or paranormal orifice of the peritoneum and the internal hernias developed through an abnormal orifice of the peritoneum [1].

The hernias of the first category most often develop quietly, under the action of peristalsis of the digestive loops trapped in a normal (omental foramen) or paranormal orifice, corresponding to a progressive detachment of normally joined peritoneal fascia during embryological development (anterior paraduodenal, pericaecal and intersigmoid hernias) [1] [2].

On clinical grounds, they are characterized by a more or less long latency period, with a more or less complete occlusive symptomatology, during which they can be diagnosed by imaging. Their revealing symptomatology can be very variable: vague sensations of epigastric heaviness, periumbilical pain, spontaneously resolving subocclusive episodes. They can obviously be revealed by an acute picture of "flat belly" occlusion as well in the event of inaugural incarceration with vascular strangulation. In imaging, it shows the existence of a hernial sac that gives the loops trapped in the cavity their overall circular appearance, corresponding to the globally spherical or ovoid volume in which they evolve [1].

Concerning the second category of internal hernias (developed through an abnormal orifice of the peritoneum), the orifice is small, with fibrous contours, inextensible, of dysembryoplastic or acquired origin (post traumatic, post inflammatory, etc.) in which a generally fairly short segment of intestine will incarcerate in a manner analogous to what may occur in certain strangulated parietal hernias. The upstream loops have a propensity to volvulate due to their fluid distension and strangulation can involve both the incarcerated intestinal segment and the upstream involuted loops [1].

The falciform ligament hernia falls into this category with transmesenteric, transomental hernias, the hernias of the gastrocolic ligament or transverse mesocolon, the hernias of the hepato-gastric ligament, the trans-meso-sigmoid and intersigmoid hernias, the hernias of the broad ligament and the perirectal hernias.

These types of internal hernia can only be diagnosed during an acute and indicative hyperalgesic episode since there is no positional abnormality of the intestinal structures before the digestive incarceration in the peritoneal "trap". This was the case of our patient under study who presented an acute symptomatology evolving for a few hours.

The revelation of these types of hernia is often early, in the case of young subjects, on average 38 years old and without prior surgery [1]. However, some late revelations despite the congenital nature of the abnormalities responsible have been noted. In the series by Zissin *et al.*, involving 11 cases, four patients aged 76 and 96 when their internal hernia was revealed by an acute picture [1]. This is the case of our patient under study who is 78 years old.

The internal hernias of the falciform ligament are exceptional and represent approximately 0.1 to 0.3% of all internal hernias. The average age is 43 years and they generally concern the small intestine. The origin of the falciform ligament defect can be congenital or inflammatory (a satellite of acute cholecystitis) or even post-surgical [1]. In the case of our patient, in the absence of particular medical and surgical history, it is probably a congenital defect.

The imaging examinations theoretically useful for the diagnosis of occlusive syndromes are the abdomen without preparation (ASP), ultrasound, Computed Tomography (CT) and magnetic resonance imaging (MRI) [10].

The ASP has long been an important examination in suspected occlusion. However, it encounters a certain number of false negatives, in particular in the case of severe occlusions when the digestive loops have an exclusively liquid content and do not allow room for the diagnosis of cause and complication. Already since 2009, the High Authority of health of France [11] had clearly concluded that ASP no longer provide any indication for mechanical occlusion and recommended performing a CT as first intention. Thus, an ASP X-ray was not performed in our patient under study.

Ultrasound has no first-line indication when faced with the suspicion of intestinal obstruction in adults. It can possibly be performed secondarily after the CT to clarify certain images [10].

MRI has no place in clinical strategies even though it has the advantage of not inducing exposure to X-rays [10].

The abdominal CT is the reference imaging examination for occlusive syndrome in adults [12]. In the context of internal hernias, it is a powerful examination, allowing an accurate diagnosis to be made in 77% of cases, with a sensitivity of 63% and a specificity of 76% [13].

The examination must be carried out with helical acquisitions in thin millimetric or sub-millimetric sections covering the volume of the abdomen and the pelvis are necessary allowing multiplanar reconstructions.

An intravenous injection of iodinated contrast product is generally recommended. If it is contraindicated (kidney failure, allergy), this must obviously be specified in the request for examination and the scanner will be less effective in the search for strangulation, even if the spontaneous hyperdensity of the digestive wall is a powerful sign in these conditions.

In the internal hernia of the falciform ligament, the scanner allows the identification of the distended loops with hydro-aeric level, whose diameter is greater than 2.5 cm. These distended loops are located in the peri-hepatic region. The scanner also finds the convergence of the mesenteric folds and the vessels in the area of stricture formed by the falciform ligament in the left lobe-lobe junction.

The scanner also makes it possible to make the diagnosis of complication by showing signs of digestive ischemia associating modifications of the digestive wall associated with modifications of the fat and the mesenteric vessels [10]. The modifications of the digestive wall are in the form either of a circumferential thickening of the intestinal wall testifying to a submucosal edema in the case of a beginner ischemia, or by a defect of parietal enhancement with a virtual wall aspect indicating a transmural infarction. A œedematous infiltration of the mesentery and turgidity of the draining veins are often associated. In the case of established infarction, there may be a high-density sero-haematic effusion between the affected loops and/or parietal pneumatosis or mesenteric-portal venous pneumatosis [10].

In the case of our patient, the topography of the distended loops as well as the study of the parietal enhancement had made it possible to evoke the diagnosis of internal hernia of the falciform ligament complicated by intestinal ischemia, thus directing towards rapid surgical procedures.

Emergency surgery is required to achieve extrication with or without intestinal resection depending on its vitality. The defect of the falciform ligament can be treated by the collapse of this ligament along the entire length of its diaphragmatic insertion in order to prevent recurrences [5]. Our patient under study had benefited from this type of treatment with unfortunately an intestinal resection-anastomosis because there were necrotic loops.

4. Conclusion

The internal hernias of the falciform ligament are exceptional, most often revealed in an array of acute intestinal obstruction. The helical CT scan is the benchmarking examination allowing us to describe the diagnosis and to detect the inherent complications. Treatment is usually surgical.

Conflicts of Interest

The authors declare no conflicts of interest regarding the publication of this paper.

References

[1] Mathias, J., Phi, I., Brunot, O., Ganne, P.-A., Laurent, V. and Regent, D. (2008) Hernies Internes. EMC (Elseiver Masson SAS), Paris, Radiodiagnostic-Appareil digestif, 33-015-A-37.

[2] Alsairafi, R. (2022) Intestinal Obstruction and Bowel Ischemia due to a Rare Left Paraduodenal Hernia: Case Report. *Surgical Science*, **13**, 28-33. https://doi.org/10.4236/ss.2022.131005

[3] Bedioui, H., Daghfous, A., Ksantini, R., Noura, K., Chabbi, F., Pteriche, F., *et al*. (2008) Hernie interne du ligament falciforme révélée par une occlusion intestinale aiguë. *La Presse Médicale*, **37**, 44-47. https://doi.org/10.1016/j.lpm.2007.03.040

[4] Wiseman, S. (2000) Internal Herniation through a Defect in the Falciform Ligament: A Case Report and Review of the World Literature. *Hernia*, **4**, 117-120. https://doi.org/10.1007/BF02353760

[5] Hasnaoui, H., Mouaqit, O., El Bachir, B., Ousadden, A., Taleb, K.A. and El Bouhaddouti, H. (2019) Hernie interne du ligament falciforme: Une cause rare d'occlusion intestinale. *Pan African Medical Journal*, **32**, Article 48. https://doi.org/10.11604/pamj.2019.32.48.17845

[6] Bills, D. and Moore, S. (2009) The Falciform Ligament and the Ligamentum Teres: Friend or Foe. *ANZ Journal of Surgery*, **79**, 678-680. https://doi.org/10.1111/j.1445-2197.2009.05050.x

[7] Li, X.P., Xu, D.C., Tan, H.Y. and Li, C.L. (2004) Anatomical Study on the Morphology and Blood Supply of the Falciform Ligament and Its Clinical Significance. *Surgical and Radiologic Anatomy*, **26**, 106-109. https://doi.org/10.1007/s00276-003-0184-0

[8] Diallo, M., Haberlay, M. and Bujor, P.C. (2022) A Rare Localisation of Intra-Abdominal Focal Fat Infarction: The Falciform Ligament. Contribution of Imagery. *Morphologie*, **106**, 115-117. https://doi.org/10.1016/j.morpho.2021.01.006

[9] Miura, D., Shindo, M. and Fukuda, Y. (2022) Hepatic Falciform *Ligament appendagitis* Evaluated by Ultrasound: A Report of 2 Cases. *Radiology Case Reports*, **17**, 4425-4430. https://doi.org/10.1016/j.radcr.2022.08.090

[10] Taourel, P., Alili, C., Pages, F., Curros Doyon, F. and Millet, I. (2013) Occlusions mécaniques: Pièges diagnostiques et éléments clés du compte rendu. *Journal de Radiologie Diagnostique et Interventionnelle*, **94**, 814-827. https://doi.org/10.1016/j.jradio.2013.03.002

[11] HAS (2009) Principales indications de la radiographie de l'abdomen sans préparation. Rapport d'évaluation technologique.

[12] Ismael, L.B.K., Mamadou, T., Bernadette, N.A., Serge, E.A., Ezechiel, A., Amos, K.B., Inza, B., Bernadin, K.K., Ibrahim, A.K., Roger, L. and Bamourou, D. (2023) An Inahbitual Etiology of Acute Intestinal Obstruction: The Giant Fecalome. *Surgical Science*, **14**, 225-230. https://doi.org/10.4236/ss.2023.143026

[13] Takeyama, N., Gokan, T., Ohgiya, Y., *et al*. (2005) CT of Internal Hernias. *RadioGraphics*, **25**, 997-1015. https://doi.org/10.1148/rg.254045035

Open Journal of Radiology, 2023, 13, 101-112
https://www.scirp.org/journal/ojrad
ISSN Online: 2164-3032
ISSN Print: 2164-3024

Image-Based Ultrasound Speed Estimation: Phantom and Human Liver Studies

Jianfeng Chen*, **Junguo Bian**, **Zuhaib Khokhar**, **Mohamed Belal**, **Emad Allam**

Department of Radiology and Medical Imaging, Stritch School of Medicine, Loyola University Medical Center, Chicago, Illinois, USA
Email: *jfchen@live.com

How to cite this paper: Chen, J.F., Bian, J.G., Khokhar, Z., Belal, M. and Allam, E. (2023) Image-Based Ultrasound Speed Estimation: Phantom and Human Liver Studies. *Open Journal of Radiology*, **13**, 101-112.
https://doi.org/10.4236/ojrad.2023.132011

Received: May 16, 2023
Accepted: June 27, 2023
Published: June 30, 2023

Abstract

Purpose: A novel image-based method for speed of sound (SoS) estimation is proposed and experimentally validated on a tissue-mimicking ultrasound phantom and normal human liver *in vivo* using linear and curved array transducers. **Methods:** When the beamforming SoS settings are adjusted to match the real tissue's SoS, the ultrasound image at regions of interest will be in focus and the image quality will be optimal. Based on this principle, both a tissue-mimicking ultrasound phantom and normal human liver *in vivo* were used in this study. Ultrasound image was acquired using different SoS settings in beamforming channels ranging from 1420 m/sec to 1600 m/sec. Two regions of interest (ROIs) were selected. One was in a fully developed speckle region, while the other contained specular reflectors. We evaluated the image quality of these two ROIs in images acquired at different SoS settings in beamforming channels by using the normalized autocorrelation function (ACF) of the image data. The values of the normalized ACF at a specific lag as a function of the SoS setting were computed. Subsequently, the soft tissue's SoS was determined from the SoS setting at the minimum value of the normalized ACF. **Results:** The value of the ACF as a function of the SoS setting can be computed for phantom and human liver images. SoS in soft tissue can be determined from the SoS setting at the minimum value of the normalized ACF. The estimation results show that the SoS of the tissue-mimicking phantom is 1460 m/sec, which is consistent with the phantom manufacturer's specification, and the SoS of the normal human liver is 1540 m/sec, which is within the range of the SoS in a healthy human liver *in vivo*. **Conclusion:** Soft tissue's SoS can be determined by analyzing the normalized ACF of ultrasound images. The method is based on searching for a minimum of the normalized ACF of ultrasound image data with a specific lag among different SoS settings in beamforming channels.

Keywords

Ultrasound Image, Normalized Autocorrelation Function (ACF), Speed of Sound (SoS)

1. Introduction

Clinical ultrasound imaging systems usually assume that the speed of sound (SoS) in soft-tissues is constant, mostly 1540 m/s, so that the sound waves in the soft-tissue can be focused by simply delaying and summing according to known geometric distances and the SoS in the tissue. Ideally, if the SoS set in beamforming channels matches the true SoS in the tissue, both the transmitted and received signals should be well aligned after applying the time delays. However, the difference between the SoS in the tissue and in the beamforming channels will cause ultrasound signal misalignment of the beamforming channels and thereby degrade both the spatial resolution and the sensitivity of ultrasound images. Moreover, if there is some in homogeneity of SoS in the soft-tissues, higher-order phase aberrations can further lead to signal misalignment after geometric delays are applied and lead to further degradation of the ultrasound image quality [1] [2] [3] [4].

A concept to estimate the SoS in soft tissue by using ultrasound was proposed by Chen *et al.* [5]. When soft tissue was scanned by an ultrasound imaging system, a series of ultrasound images were created by using different SoS settings in beamforming channels. Then, an image quality function that is indicative of image quality at a specific region of interest (ROI) was computed. That function could exhibit a minimum or maximum value when the SoS setting in beamforming channels equals a true SoS in the tissue. A method to select the SoS automatically in order to improve lateral resolution in the resulting image was developed by Napolitano *et al.* [4] [6] [7]. This is done by analyzing the spatial frequency data of images reconstructed with various sound speeds. The main limitation of the method is that the image must contain an isolated feature. This concept was then applied to photo acoustic tomography of soft tissues [8] in order to obtain an average SoS that can maximize the image sharpness. This method eliminates the need of a priori knowledge, such as the geometry of a calibration block or a reference image for comparison.

In this paper we propose a method based on the normalized autocorrelation function (ACF) of image data for averaged SoS estimation. The method works well under weaker constraints, *i.e.*, no assumption of isolated image features, whether for speckle, the appearance of texture due to ultrasound scattering from a set of diffuse small scattering structures within a specific tissue, or the specular reflector with structure scale larger than the ultrasound wavelength. This study is organized as follows: In Section 2, a method based on the normalized ACF of image data for averaged SoS is presented; in Section 3, the experiments set up for both a tissue mimicking phantom and healthy liver images *in vivo* are described; in Section 4, the test results are discussed and summarized. Section 5 presents the final conclusions.

2. Method

In our study, an ultrasound tissue mimicking phantom (Multipurpose Phantom Model 539, ATS Laboratories Incorporated, Bridgeport, CT) and a normal human liver were used in this study. A GE LOGIQ E9 scanner with a ML6-15 linear array transducer at 10 MHz and C1-6 curved array transducer at 3.5 MHz were used. As shown in Figure 1, a series of ultrasound images were generated by using different SoS settings in beamforming channels. The SoS settings were ranged from 1420 m/sec to 1620 m/sec. In our phantom study, two ROIs were selected among those ultrasound images, as shown in Figure 2. One was located in a fully developed speckle area with an image size of 150 × 50 pixels, while other contained a specular reflector with the same size of 150 × 50 pixels using the ML6-15 linear array. In our human liver study, two ROIs with the same size

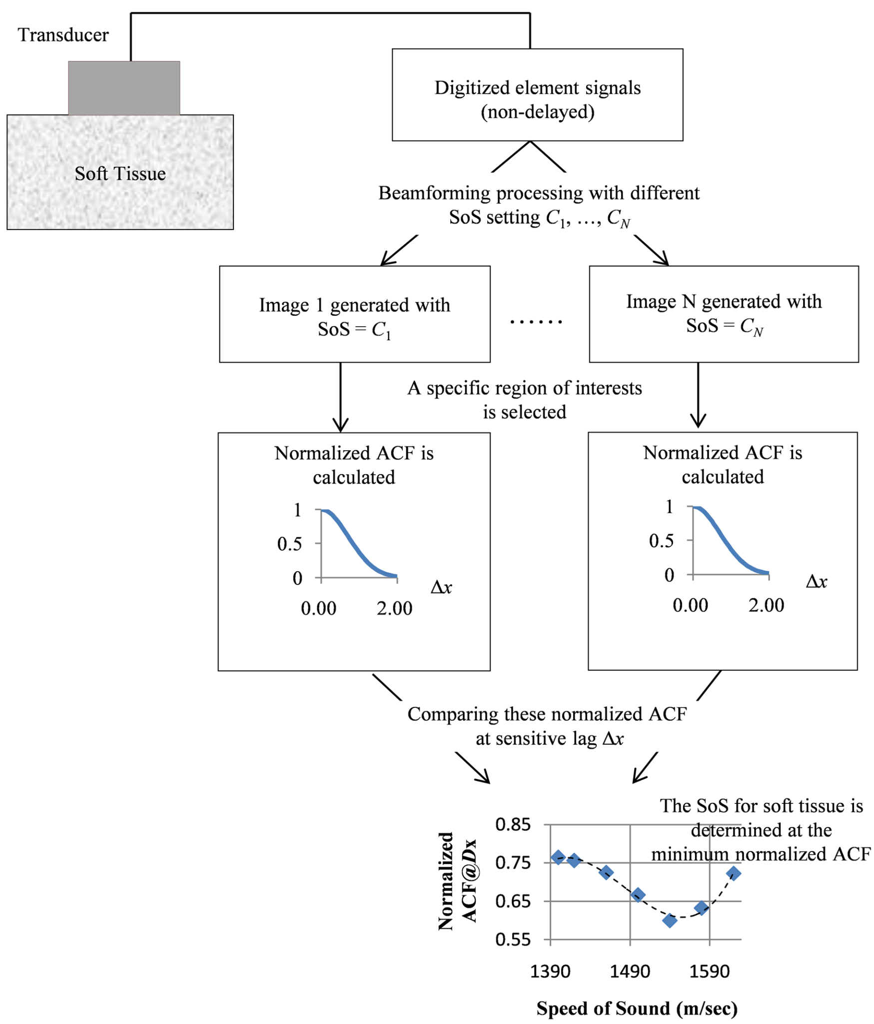

Figure 1. Block diagram of the image-based SoS estimation method.

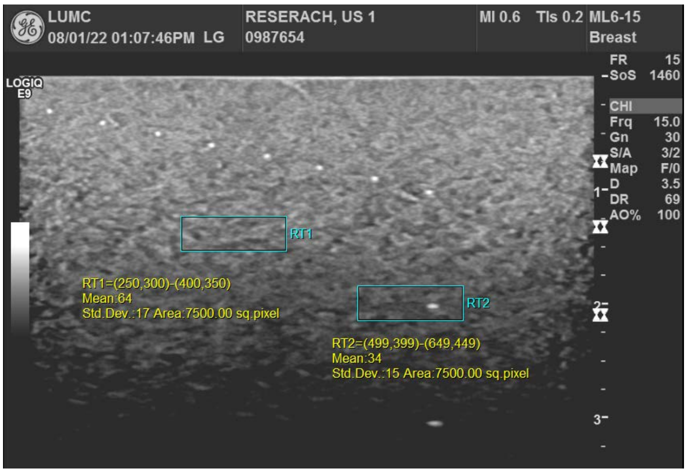

Figure 2. Two ROIs were selected on a typical ultrasound phantom image. One region contains fully developed speckle, while the other region contains a specular reflector.

of 200 × 50 pixels (ML6-15 linear transducer) and 100 × 100 pixels (C1-6 curved array transducer) were selected respectively, one was within a fully-developed speckle area, while the other contained some specular structures as shown in Figure 3 and Figure 4. Image pixel size was 0.089 mm for the ML6-15 linear array and 0.25 mm for the C1-6 curved array transducer.

Subsequently, we can evaluate the image quality by using a normalized ACF of image data over these ROIs. Here the normalized ACF is defined by

$$\mathrm{ACF}(\Delta x)=\frac{\sum_{i=1}^{M}\sum_{j=1}^{N}\left[\left(I(x_i,y_j)-\langle I\rangle\right)*\left(I(x_i+\Delta x,y_j)-\langle I\rangle\right)\right]}{\sum_{i=1}^{M}\sum_{j=1}^{N}\left[I(x_i,y_j)-\langle I\rangle\right]^2}$$

where

$I(x_i,y_j)$ is the ultrasound image signal intensity at location (x_i,y_j),

x is in the lateral direction and y is in the depth direction,

$M\times N$ is the total number of data pairs $I(x_i,y_j)$ and $I(x_i+\Delta x,y_j)$ in aROI,

Δx is the lag distance between two positions (x_i,y_j) and $(x_i+\Delta x,y_j)$ in the lateral direction, which is perpendicular to the depth direction ofultrasound image, and

$\langle I\rangle$ is the mean of image intensity within ROI and is given by

$$\langle I\rangle=\frac{\sum_{i=1}^{M}\sum_{j=1}^{N}I(x_i,y_j)}{M\times N}.$$

The shape of a typical normalized ACF for ultrasound image data is approximately Gaussian, as shown in Figure 5(a). The steepest slope of the normalized ACF, corresponding to a second derivative of zero, will be the most sensitive point where a change in lag will result in the largest change in ACF, as shown in Figure 5(b). If the shape of the normalized ACF is given by $y=\mathrm{e}^{-a\Delta x^2}$, then based on $y''=0$, we have the most sensitive lag, Δx, which satisfies the following equation:

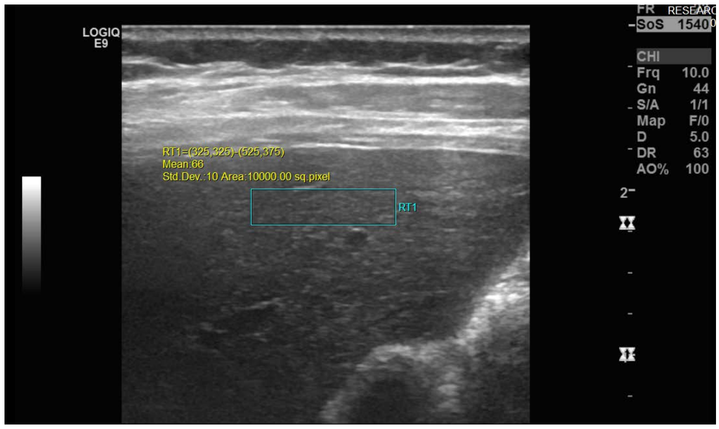

(a)

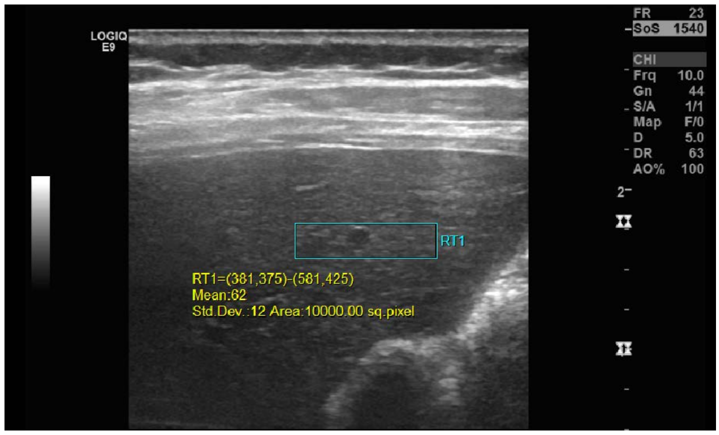

(b)

Figure 3. Two ROIs were selected on a typical ultrasound human liver image with a ML6-15 linear array transducer. One region contains a fully developed speckle, as shown in (a), while the other region contains some specular structures, as shown in (b).

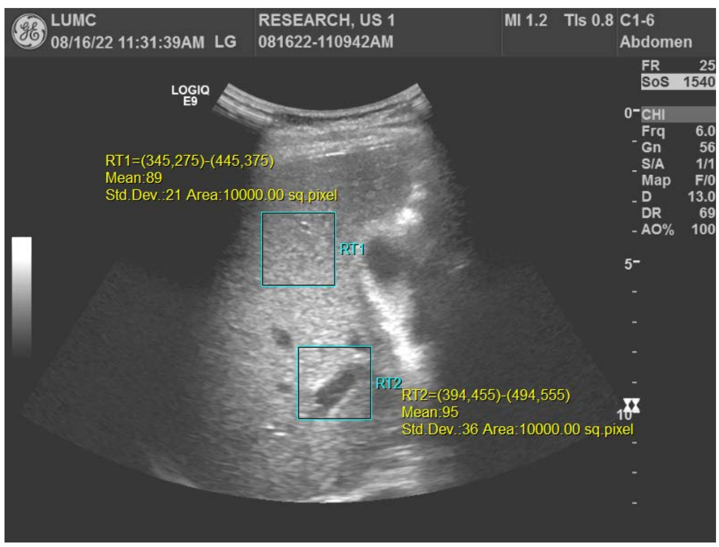

Figure 4. Two ROIs were selected on a typical ultrasound human liver image with a C1-6 curved array transducer. One region contains a fully developed speckle, while the other region contains some specular structures.

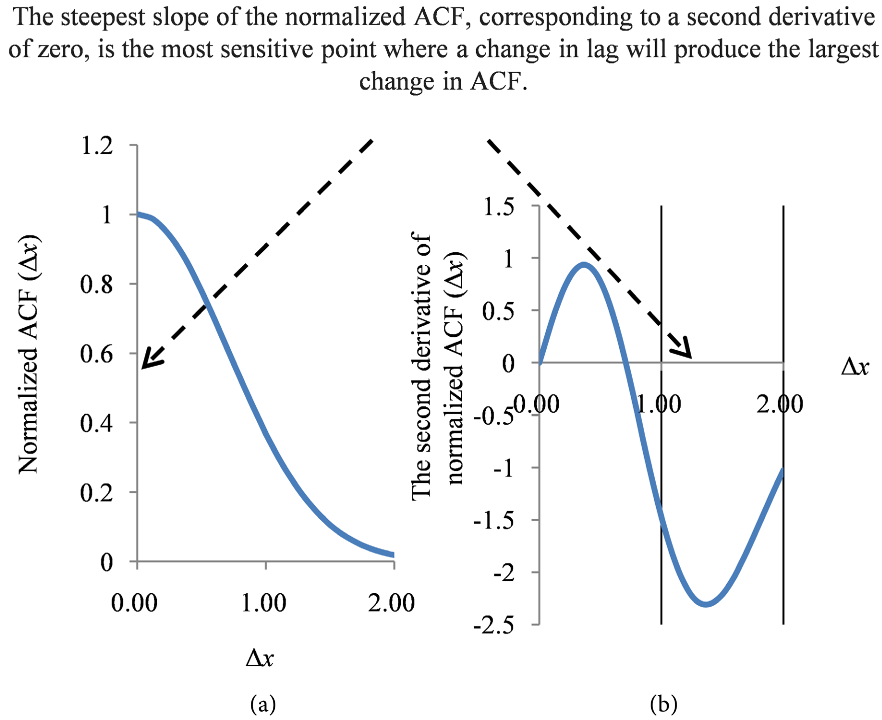

Figure 5. The shape of a typical normalized ACF of ultrasound image data is approximately a Gaussian function as shown in (a). The steepest slope of the normalized ACF, corresponding to a second derivative of zero, is the most sensitive point where a change in lag will produce the largest change in ACF, as shown in (b).

$$1-2a(\Delta x)^2 = 0$$

The value of normalized ACF for the most sensitive lag is given by $y = e^{-1/2} = 0.6065$. Here a is the ACF parameter, which not only depends on the spatial resolution of ultrasound image system, but also depends on the ultrasound scattering structure, such as speckle or specular structures. In our study, the most sensitive lag of the normalized ACF were typically in the range of 0.5 mm to 1.0 mm for the images acquired with a ML6-15 transducer, and in the range of 0.5 mm to 2.0 mm for the images acquired with a C1-6 transducer.

3. Results

In our phantom study, the phantom images were acquired using a GE LOGIQ E9 scanner with a ML6-15 linear array transducer. The values of normalized ACF with different lays as well as different SoS settings were computed. When the ROI was in a well-developed speckle region as shown in Figure 2, a lag of 0.534 mm was chosen in order to obtain a minimum value of the normalized ACF reaching just below 0.6065 for at least one particular SoS setting. The values of normalized ACF for a lag of 0.534 mm changed with different SoS settings as shown in Figure 6(a). Similarly, when the ROI contained a specular reflector region, also as shown in Figure 2, a lag of 0.75 mm was chosen in order to obtain a minimum value of the normalized ACF reaching just below 0.6065 for at least

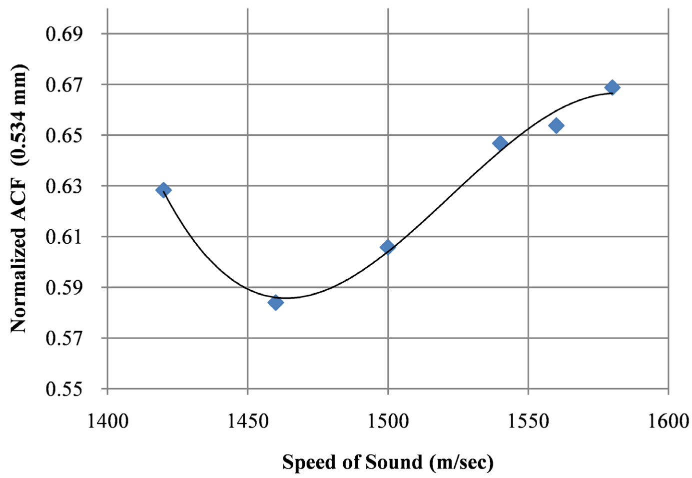

(a)

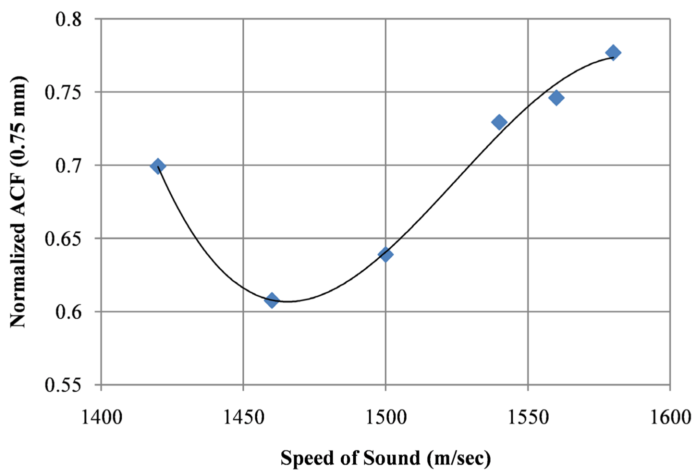

(b)

Figure 6. In our phantom experiment, the normalized ACF with a lag of 0.534 mm as a function of SoS setting for a fully developed speckle is given in (a), while the normalized ACF with a lag of 0.75 mm as a function of SoS setting for a region containing a specular reflector is given in (b).

one particular SoS setting. The results of normalized ACF values with a lag of 0.75 mm in that region varied with different SoS settings are shown in **Figure 6(b)**. Both results show that the minimum value of the normalized ACF is located at SoS = 1460 m/sec, which is very close to the SoS specification of 1450 m/sec provided by the phantom manufacturer. The results demonstrate that both speckle and specular regions can be used to assess SoS in soft tissue. The values of the normalized ACF changed with SoS settings from 1450 m/sec to 1580 m/sec are given in **Table 1**. The results show that the normalized ACF of images containing specular structures, such as the point target here, may be more sensitive to the SoS setting and may provide better SoS estimation results than the ACF of images containing only speckle structures.

In the next step, the ultrasound images of normal human livers were acquired

Table 1. The values of the normalized ACF changed with SoS settings from 1450 m/sec to 1580 m/sec in the ROI containing the fully developed speckle and the specular structures.

SoS settings (m/sec)	1420	1460	1500	1540	1560	1580
Value of Normalized ACF from speckle region	0.6383	0.5839	0.6058	0.6467	0.6537	0.6688
Value of Normalized ACF from specular structure region	0.6992	0.6075	0.639	0.7294	0.746	0.7768

using the same ultrasound scanner with a ML6-15 transducer. The ROIs containing the speckle area as well as some specular structures in the liver image were selected as shown in **Figure 3**. The values of normalized ACF of image data with different lags and different SoS settings were computed. For these images acquired with the ML6-15 transducer, a lag of 0.534 mm was selected in order to get the minimum values of the normalized ACF calculated from a speckle image area reached just below 0.6065, and a lag of 1.10 mm was selected in order to get the minimum values of the normalized ACF calculated from a specular image area reach just below 0.6065. **Figure 7(a)** is the result of the normalized ACF values with a lag of 0.534 mm at different SoS settings, while **Figure 7(b)** is the result of the normalized ACF values with a lag of 1.1 mm at different SoS settings. Both results show that the minimum value of the normalized ACF with the lags of 0.534 mm and 1.10 mm were located at SoS = 1540 m/sec, which is close to the SoS of normal human liver *in vivo*.

Finally, ultrasound images of normal human livers were acquired using the same ultrasound scanner with a C1-6 curved array transducer. As shown in **Figure 4**, the selected ROIs contain speckles as well as some specular structures in the liver images. The values of normalized ACF of image data with different lags and different SoS settings were computed. For these images acquired with a C1-6 curved array transducer, a lag of 1.5 mm was chosen to obtain the minimum value of normalized ACF computed from the speckle image area, which was just below 0.6065, and a lag of 3.0 mm was chosen to get the minimum value of the normalized ACF computed from the specular image area, which was just below 0.6065. **Figure 8(a)** is the result of normalized ACF values with a lag of 1.5 mm at different SoS settings, while **Figure 8(b)** is the result of normalized ACF values with a lag of 1.1 mm at different SoS settings. Both results show that the minimum values of the normalized ACF with lags of 1.5 mm and 3.0 mm are also located at SoS = 1540 m/sec, which is consistent with the results using linear array transducers and close to the SoS of normal human liver *in vivo*.

4. Summary and Discussion

In this paper, a novel image-based method is presented to determine the SoS of soft tissues. The method is based on searching for a minimum of the normalized

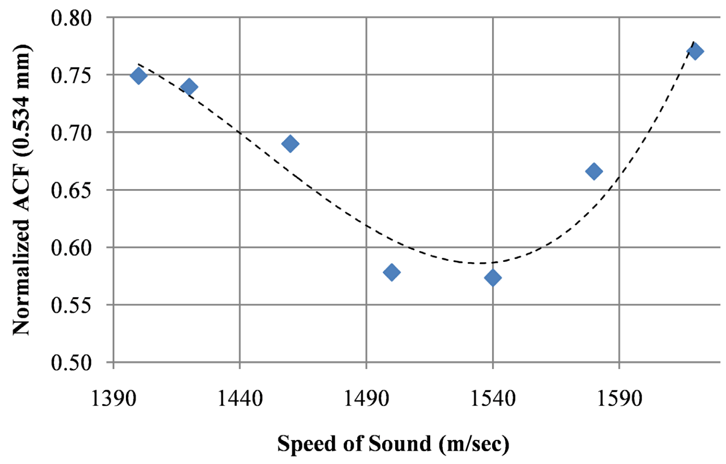

(a)

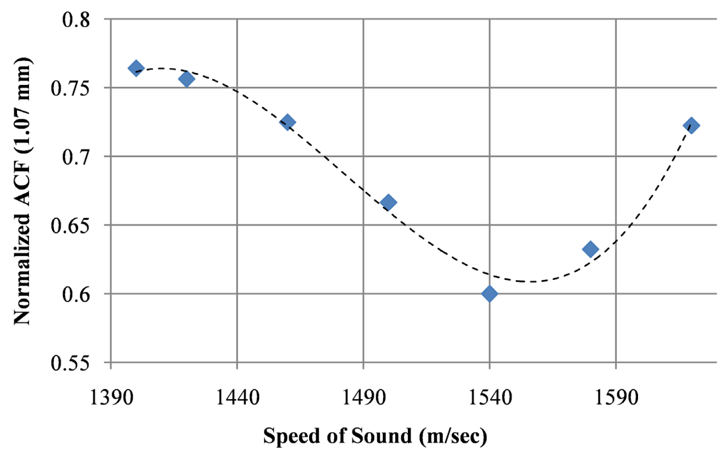

(b)

Figure 7. In our clinical study with a ML6-15 linear array transducer, the normalized ACF with a lag of 0.534 mm as a function of SoS setting for a fully developed speckle is given in (a), while the normalized ACF with a lag of 1.10 mm as a function of SoS setting for a region containing a specular reflector is given in (b).

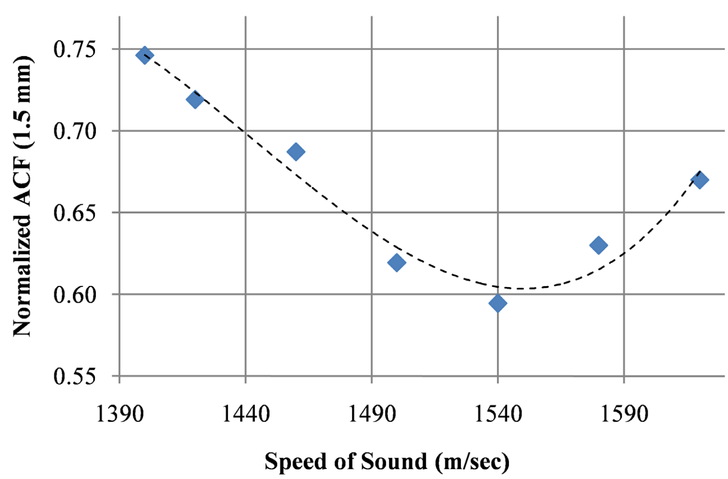

(a)

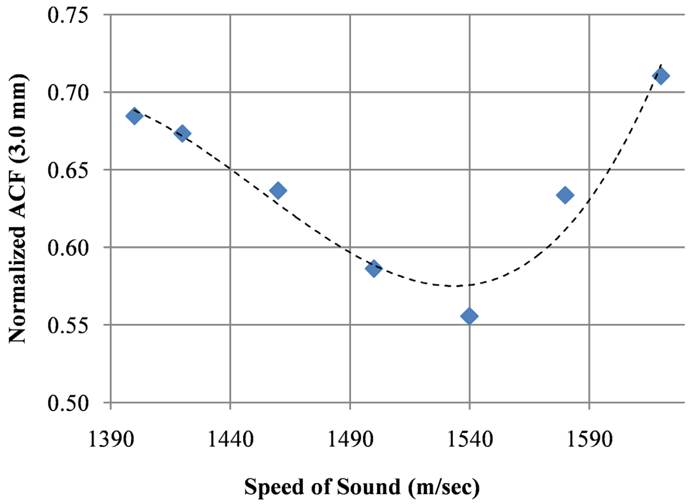

(b)

Figure 8. In our clinical study with a C6-1 curved array transducer, the normalized ACF with a lag of 1.5 mm as a function of SoS setting for a fully developed speckle is given in (a), while the normalized ACF with a lag of 3.0 mm as a function of SoS setting for a region containing a specular reflector is given in (b).

ACF of ultrasound image data with a specific lag among different SoS settings in beamforming channels. The proposed method was validated by imaging a tissue mimicking phantom and normal human liver tissue *in vivo* using a 10 MHz linear array transducer and a 3.5 MHz curved array transducer. If a similar time delay formula can be established for specific transducers, the principle of the method can be generalized to other types of transducers. Our experimental results also show that the lateral resolution of ultrasound images can be noticeably improved if the SoS setting in beamforming channels is close to the real SoS in soft tissues. This means that the minimized ACF value corresponds to maximized image sharpness.

Our method is based on the relative change in normalized ACF of ultrasound image data within a specific ROI and does not require any prior knowledge or assumptions about the ultrasound image, so it is more robust than other methods using RF data processing, which often require adding assumptions such as a reflector or a reference image to find the appropriate time delay.

In real clinical cases, a series of ultrasound images with different SoS settings in beamforming channels should be acquired in a short period of time to avoid changes in the imaging area due to transducer motion and patient motion (e.g. breathing motion). A better approach is to acquire just one set of RF data and then process the same set of RF data in beamforming with different SoS settings to create a series of images. Based on these series of images, our method can then be applied to determine SoS in soft tissues.

Our current study assumes that the effective SoS in soft tissues is uniform, but in reality, the SoS may vary at different locations, such as the body walls with multiple layers of fat and muscle, which may bias the estimation of SoS in the liver. A method including correction for fat/muscle layer effects has been studied and discussed [9]. The thickness of the fat and muscle layers can be measured by doctors using routine ultrasound. The average SoS used in the calculations could be 1450 m/sec in fat and 1575 m/sec in muscle [10]. Then, in a multi-layer medium, the SoS of different layers is given by

$$\frac{d_{total}}{SoS_{total}} = \frac{d_{muscle}}{SoS_{muscle}} + \frac{d_{fat}}{SoS_{fat}} + \frac{d_{liver}}{SoS_{liver}}$$

where

d_{total} is the depth of ROI, which is used to calculate the normalized ACF,

d_{fat} is the thickness of the fat layer,

SoS_{fat} is the SoS in the fat,

d_{muscle} is the thickness of the muscle layer, and

SoS_{muscle} is the SoS in the muscle.

If $d_{liver} = d_{total} - d_{fat} - d_{muscle}$, and SoS_{liver} is the SoS in the liver, we can determine

$$SoS_{liver} = \frac{d_{liver}}{\frac{d_{total}}{SoS_{total}} - \frac{d_{fat}}{SoS_{fat}} - \frac{d_{liver}}{SoS_{liver}}}$$

In routine clinical examinations, the situation may be more complicated, such as the SoS may not be uniform in soft tissues, strong phase aberration and other image artifacts can degrade the image quality and consequently bias measurement results. The movement of body tissues, which may vary the ROI used to compute the normalized ACF, can produce additional measurement errors.

5. Conclusion

In this paper, a novel image-based method to determine SoS of soft tissue is proposed and validated on both a tissue mimicking phantom and human liver tissue *in vivo* using both linear and curved array transducers. The method is based on searching for a minimum of the normalized ACF of ultrasound image data with a specific lag among different SoS settings in beamforming channels.

Conflicts of Interest

The authors declare no conflicts of interest regarding the publication of this paper.

References

[1] Chen, Q. and Zagzebski, J. (2004) Simulation Study of Effects of Speed of Sound and Attenuation on Ultrasound Lateral Resolution. *Ultrasound in Medicine and Biology*, **30**, 1297-1306. https://doi.org/10.1016/j.ultrasmedbio.2004.07.012

[2] Cho, M.H., Kang, L.H., Kim, J.S. and Lee, S.Y. (2009) An Efficient Sound Speed Es-

timation Method to Enhance Image Resolution in Ultrasound Imaging. *Ultrasonics*, **49**, 774-778. https://doi.org/10.1016/j.ultras.2009.06.005

[3] de Moura, H.L., de Oliveira Silva, V., Guarneri, G.A., Guerreiro, M.T.L., Passarin, T.A.R., Pires, G.P. and Pipa, D.R. (2020) Image-Based Ultrasound Speed Estimation in Isotropic Materials. *IEEE Sensors Journal*, **20**, 12903-12913. https://doi.org/10.1109/JSEN.2020.3002853

[4] Napolitano, D., *et al*. (2006) Sound Speed Correction in Ultrasound Imaging. *Ultrasonics*, **44**, e43-e46. https://doi.org/10.1016/j.ultras.2006.06.061

[5] Chen, J., Yao, L. and Von Behren, P. (1997) Ultrasound System for Estimating the Speed of Sound in Body Tissue. US Patent, Patent Number: 5638820.

[6] Ali, R., Telichko, A.V., Wang, H.J., Sukumar, U.K., Vilches-Moure, J.G., Paulmurugan, R. and Dahl, J.J. (2022) Local Sound Speed Estimation for Pulse-Echo Ultrasound in Layered Media. *IEEE Transactions on Ultrasonics, Ferroelectrics, and Frequency Control*, **69**, 500-511. https://doi.org/10.1109/TUFFC.2021.3124479

[7] Jakovljevic, M., Hsieh, S., Ali, R., Kung, G.C.L., Hyun, D. and Dahl, J.J. (2018) Local Speed of Sound Estimation in Tissue Using Pulse-Echo Ultrasound: Model-Based Approach. *Journal of the Acoustical Society of America*, **144**, 254-266. https://doi.org/10.1121/1.5043402

[8] Treeby, B.E., Varslot, T.K., Zhang, E.Z., Laufer, J.G. and Beard, P.C. (2011) Automatic Sound Speed Selection in Photoacoustic Image Reconstruction Using an Autofocus Approach. *Journal of Biomedical Optics*, **16**, 090501. https://doi.org/10.1117/1.3619139

[9] Imbault, M., Faccinetto, A., Osmanski, B., Tissier, A., Deffieux, T., Gennisson, J., Vilgrain, V. and Tanter, M. (2017) Robust Sound Speed Estimation for Ultrasound-Based Hepatic Steatosis Assessment. *Physics in Medicine & Biology*, **62**, 3582-3598. https://doi.org/10.1088/1361-6560/aa6226

[10] Azhari, H. (2010) Appendix A: Typical Acoustic Properties of Tissues Basics of Biomedical Ultrasound for Engineers. Wiley, New York, 313-314. https://doi.org/10.1002/9780470561478.app1

Scientific Research Publishing

Open Journal of Radiology, 2023, 13, 113-123
https://www.scirp.org/journal/ojrad
ISSN Online: 2164-3032
ISSN Print: 2164-3024

Correlation between Ultrasound Aspects of Fibrosis and Fibroscan Outcomes of Patients with Chronic Hepatitis B Virus

Bénilde Marie-Ange Tiemtore-Kambou[1,2], Adjirata Koama[1*], Alice Guingane[2,3], Maimouna Payété Gynette Belem[1], Nina Astrid Ndé Ouedraogo[1,2], Madina Napon[2,4], Ousséni Diallo[2,5], Claudine Lougue[2,4], Rabiou Cisse[4,5]

[1]Department of Medical Imaging and Interventional Radiology of the Teaching Hospital of Bogodogo, Bogodogo, Burkina Faso
[2]Training and Research Department in Health Sciences of Joseph Ki Zerbo University of Ouagadougou, Ouagadougou, Burkina Faso
[3]Department of Internal Medicine, Endocrinology and Metabolic Diseases of the Teaching Hospital of Bogodogo, Bogodogo, Burkina Faso
[4]Department of Radiology, Teaching Hospital of Charles de Gaulle, Ouagadougou, Burkina Faso
[5]Department of Radiology, Teaching Hospital of Yalgado Ouédraogo, Ouagadougou, Burkina Faso

Email: kbenildema@yahoo.fr, *adjikoama@gmail.com, aliceguingane@yahoo.fr, ginettebelem@gmail.com, ninawed@yahoo.fr, naponma@yahoo.fr, odiallo75@yahoo.fr, claudinelougue@yahoo.fr, cissrab@gmail.com

How to cite this paper: Tiemtore-Kambou, B.M.-A., Koama, A., Guingane, A., Belem, M.P.-G., Ouedraogo, N.A.N., Napon, M., Diallo, O., Lougue, C. and Cisse, R. (2023) Correlation between Ultrasound Aspects of Fibrosis and Fibroscan Outcomes of Patients with Chronic Hepatitis B Virus. *Open Journal of Radiology*, **13**, 113-123.
https://doi.org/10.4236/ojrad.2023.132012

Received: November 28, 2022
Accepted: June 27, 2023
Published: June 30, 2023

Abstract

Background: The assessment of liver fibrosis is an essential part of the follow-up of patients with chronic HBV. Ultrasound and fibroscan are two commonly used non-invasive examinations and the purpose of this study is to assess the correlation between the results of these two examinations in the assessment of liver fibrosis. **Methodology**: This was a descriptive and analytical cross-sectional study with retrospective collection over a period of 30 months from January 01, 2018 to June 30, 2020 on the correlation between the ultrasound aspects and the results of the fibroscan of patients with chronic carriers of Hepatitis B virus at the Teaching Hospital of Bogodogo and at the faith-based health center CANDAF. **Results**: A total of 85 patients with fibrosis were collected. The 30 - 40 age group was the most represented (41.18%), with a male predominance of 52.94%. The patients with a married life were the most represented (77.64%), the social stratum the most represented were the middle managers (32.94%). University level was predominant among education levels (45.64%). The personal history was traditional circumcision (34.12%), excision (21.18%), manicure (16.47%). The circumstances of the findings were blood donation (34.12%), screening (21.18%), fortuitous findings (16.47%). The association between echostructure and fibrosis on the fibroscan scan was significant (homogeneous hyperechoic echostructure p = 0.0028 and granular echostructure p = 0.0001). Fibrosis on scans had a significant association with liver contour (Regular contours p = 0.0009 and p = 0.0002). Fibrosis on CT scan had a significant association for the diagnosis of fibrosis on ultrasound (p = 0.0002 for hepatic steatosis and cirrhosis and p = 0.0013 for hepatic dysmorphia), on the other hand, no significant association for hepatomegaly (p = 0.8883). **Conclusion**: Detecting the presence of fibrosis and monitoring its progression improves the management of patients with chronic liver disease. Ultrasound scans and fibroscan are complementary in the follow-up of patients with chronic HBV.

Keywords

Fibrosis, HBV, Ultrasound, Fibroscan, Correlation

1. Introduction

Viral hepatitis B (HBV) is a major public health problem in sub-Saharan Africa with approximately 65 million chronic carriers and 56,000 deaths per year [1]. The severity of liver damage conditions both the prognosis and the therapeutic indications during chronic hepatitis [2]. The clinical expression of the natural history of this infection is very variable, ranging from simple inactive carriage to chronic active hepatitis with progressive fibrosis that can lead to cirrhosis, which in its turn can be complicated by hepatocellular carcinoma [2] [3]. In rare situations, hepatocellular carcinoma occurs in a non-cirrhotic liver [4]. Fibrosis is an essential element to monitor in the search for complications of viral hepatitis B [3]. Indeed it is part of the definition of cirrhosis, which is a diffuse process defined by mutilating fibrosis (destroying the normal lobular architecture of the liver), delimiting hepatocyte nodules of abnormal structure called regeneration nodules [5]. Liver biopsy is the gold standard for the diagnosis of liver fibrosis. However, it has the disadvantage of being an invasive procedure with risks of morbidity (0.3% to 0.6%) and mortality (0 to 0.05%) [6] [7]. This invasive examination cannot therefore be repeated in the context of monitoring the evolution of liver fibrosis, hence the development of non-invasive alternatives with blood and morphological tests. Elastometry or fibroscan is a promising and reproducible non-invasive approach to the quantification of fibrosis [8] [9] [10]. Ultrasound is the first-line imaging test used in the follow-up of patients infected with HBV. The advantages of ultrasound are its low cost, reproducibility, non-invasiveness and innocuousness, which can be repeated at will. However, the diagnostic performance of ultrasound for the diagnosis of hepatic fibrosis is insufficient, and its diagnostic accuracy depends on the signs sought [11]. Despite its disadvantages, ultrasound is the most economically and geographically accessible examination in our working context [12]. The aim of our work is to study the correlation between the ultrasound aspects of fibrosis and the results of the fibroscan of chronic carriers of the hepatitis B virus.

2. Material and Methods

This was a descriptive and analytical cross-sectional study with retrospective and prospective collection over a 30-month period from January 1, 2018 to June 30, 2020. Our study population was all chronic HBV infected patients to whom has been done an ultrasound scan during our study period at the teaching hospital of Bogodogo and at the CANDAF faith-based centre and who subsequently underwent a fibroscan. For each patient we noted age, sex, profession, marital status, ultrasound data including right liver, left liver, segment IV and segment I sizes, liver edge and its echotexture, portal vein trunk diameter, permeability and flow direction, splenomegaly and ascites presence or not. We also noted fibrosis score on fibroscan. Data sources were ultrasound reports, fibroscan reports and patient phone calls. Data were collected on an electronic collection form installed on an android smartphone. Data analysis was done on a microcomputer using Stata software version 17. To compare our results, we used the chi-square statistical test; the threshold of $p < 0.05$ was retained as statistically significant.

The following ultrasound signs of cirrhosis and extensive fibrosis were used in this study: hepatomegaly: right liver greater than 150 mm, measured anterior to the right kidney on the medio-clavicular line; diffuse micronodular liver: granular heterogeneous echotexture made up of micronodules less than 3 mm; diffuse macronodular liver: nodular heterogeneous echotexture made up of nodules less than 3 to 20 mm, generally hyperechoic; hepatic dysmorphia: change in hepatic proportions with right liver atrophy (size less than 120 mm), segment IV atrophy (size less than 30 mm), left liver hypertrophy (size greater than 120 mm) and segment I hypertrophy (size greater than 15 mm); portal hypertension: diameter of the portal trunk measured at the hepatic hilum greater than 12 mm +/− hepatofugal flow. Portal hypertension syndrome: dilatation of the portal trunk associated with splenomegaly and/or ascites.

Fibroscan score: Elasticity score > 10 kpa (likely F3-F4: severe fibrosis); 7 kpa < elasticity score ≤ 10 kpa (likely F1-F2: moderate fibrosis); 2.5 kpa ≤ elasticity score ≤ 7 kpa (F0-F1: absent or minimal fibrosis).

The secrecy and confidentiality of the information was respected. The protocol was submitted to the Ethics National Committee of Burkina Faso for biomedical research and was approved by deliberation n° 2021-07-180.

3. Results

A total of 993 ultrasounds were performed in chronic HBV infected patients and 289 ultrasounds were abnormal. Fibrosis was found in 283 ultrasound results but only 85 patients with both ultrasound and fibroscan agreed to participate in the study. Figure 1 shows the flow-chart of the ultrasound and fibroscan results.

Thus we included 85 patients with both ultrasound and fibroscan in this study. The mean age of the patients was 38 years with extremes of 19 and 69 years. The age range 30 - 40 years was represented by 41.18%. There was a male predominance with 45 patients and the sex-ratio was 1.12. Middle managers

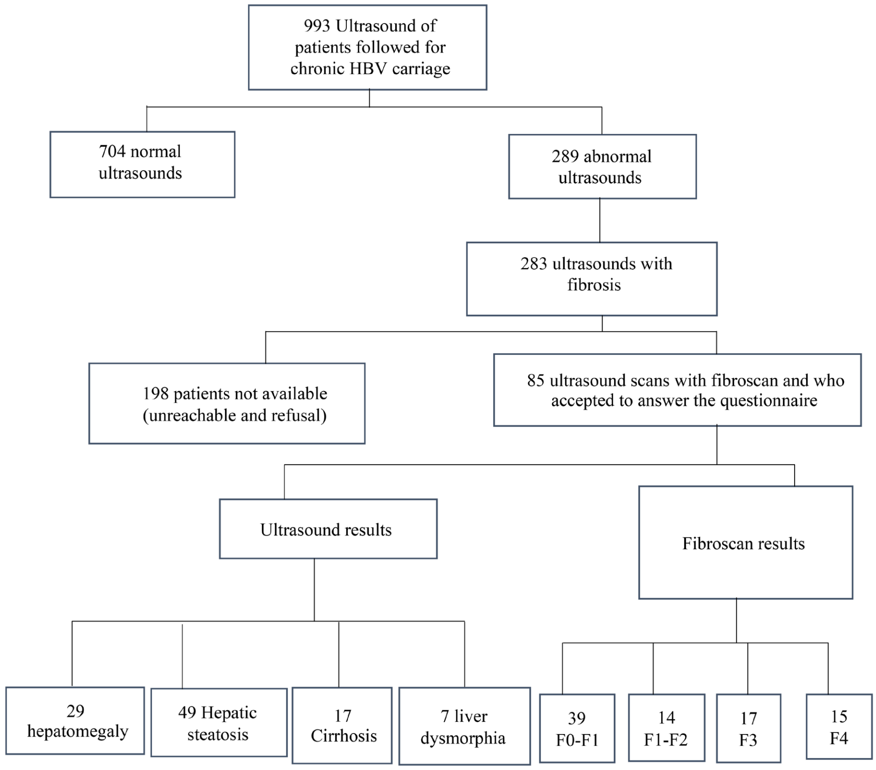

Figure 1. Flow chart of ultrasound and fibroscan results in chronic HBV infected patients.

were represented at 32.94% (N = 85) followed by informal sector actors at 17.65% (N = 85). Patients with a higher education were represented at 45.88% followed by those with secondary education at 28.4%. The majority of patients (85.88% or 73) lived in urban areas and follow-up was mainly carried out in a public facility (44.71%), followed respectively in a religious facility (27.06%), then private facility (22.35%) and the provinces (5.88%). In our study population, all fibroscan examinations were prescribed by a hepato-gastroenterologist (100%). Regarding alcohol consumption as another risk factor for fibrosis, n = 21 patients or 24.71% claimed to be regular consumers of alcohol in unspecified quantities.

According to the quality criteria of the ultrasound reports, some elements had not been filled in. Table 1 gives the distribution of the dimensions of the liver filled in on the different ultrasound reports. Average size of right liver was 137.706 mm with extremes of 45 and 177 mm. That of left liver was 96.417 mm with extremes of 80 and 122 mm. Those of segment 4 and segment 1 were respectively 36.945 and 38 with extremes of 21 and 51 mm and 9 and 55 mm.

Liver edge was recorded in the entire study population. The edge was regular with a frequency of 78.82% (n = 67) and irregular with a frequency of 21.18% (n = 18).

Liver echotexture was homogeneous hyperechoic in 66 patients (77.65%), granular in 18 patients (21.18%) and micronodular in 4 patients (4.71%).

Table 1. Distribution of chronic hepatitis B virus infected patients according to liver size (N = 85).

Variables	effective	Averagesize	Standard deviation	Min	Max
Right liver	85	137.706	19.11	45	177
Left liver	24	96.417	10.521	80	122
Segment IV	73	36.945	7.137	21	51
Segment I	3	38	25.239	9	55

Hepatic steatosis appeared to be the most frequent ultrasound diagnosis (n = 49 or 57.65%) in these patients followed by hepatomegaly (n = 29 or 34.12%), cirrhosis (n = 17 or 20%) and dysmorphia (n = 7 or 0.08%).

The average time interval between ultrasound and fibroscan was 6 days, the maximum was 120 days and the minimum was 1 day for patients who had both examinations.

On fibroscan, 39 patients or 45.88% had a score between F0-F1, 14 patients or 16.47% between F1-F2, 17 patients or 20% had a score at F3 and 15 patients 17.65% had a score at F4. Figure 2 shows fibroscan score frequency in our study population.

Association tests between liver echotexture findings on ultrasound and fibrosis on fibroscan showed a significant association between hyperechogeneous and granular liver with fibrosis. Respectively p-value was 0.2% and 0.01% and the strength of this association was 8.92 and 19.36.

Table 2 shows the association tests.

Association tests between final diagnosis on ultrasound and fibrosis on fibroscan showed a significant association between steatosis, cirrhosis, dysmorphia and fibrosis with a respective p-value of 0.02%, 0.02% and 0.13%. There was no significant association between hepatomegaly and fibrosis (p-value = 88%). Table 3 shows the association tests.

The association tests between liver edge on ultrasound and fibrosis on fibroscan showed a positive association between liver edge and the presence of fibrosis. There was significant association between irregular edge of liver on ultrasound and fibrosis with p-value of 0.02%. There was also significant association between regular edge of liver on ultrasound and fibrosis with p-value of 0.09%. The strength of this association was 11 for regular edge and 13 for irregular edge.

Table 4 shows the association tests.

Figure 3 showed correlation between ultrasound diagnosis of cirrhosis and the advanced fibrosis (F4) on fibroscan in a 28-year-old patient with chronic hepatitis.

4. Discussion

The young age of chronic HBV infected patients seen on ultrasound has also been found in several sub-regional [1] [10] and national [13] [14] studies. However,

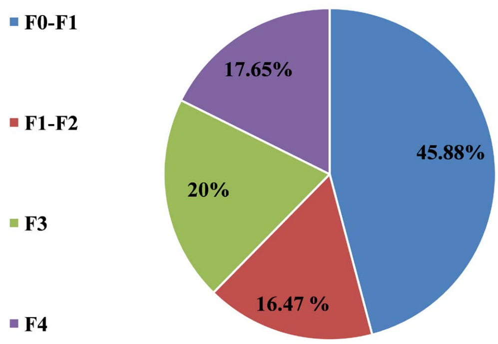

Figure 2. Fibroscan score frequency (N = 85).

Table 2. Correlation between liver echotexture and fibrosis on fibroscan in patients with chronic hepatitis B virus.

Variables	Fibrosis score				
Homogeneous hyperechogenous	**Fibrosis −**	**Fibrosis +**	**Total**	**Odd ratio**	**P-value**
Yes	36	30	66	8.92	0.0028
No	3	16	19		
Granular					
Yes	0	18	18	19.36	0.0001
No	39	28	67		
Micronodular					
Yes	1	3	4	0.74	0.3906
No	38	43	81		

*Fibrosis (+) = F1-F2, F3, F4; *Fibrosis (−) = F0-F1.

Table 3. Correlation between ultrasound diagnoses and fibroscan results of chronic hepatitis B virus infected patients.

Variables	Fibrosis score				
Hepatomegaly	**Fibrosis −**	**Fibrosis +**	**Total**	**Odd ratio**	**P-value**
Yes	13	16	29	0.02	0.8883
No	26	30	56		
Hepatic steatosis					
Yes	31	18	49	14.08	0.0002
No	8	28	36		
Cirrhosis					
Yes	1	16	17	13.69	0.0002
No	38	30	68		
Dysmorphia					
Yes	3	4	7	11.07	0.0013
No	36	42	78		

*Fibrosis (+) = F1-F2, F3, F4; *Fibrosis (−) = F0-F1.

Table 4. Correlation between the appearance of liver edges on ultrasound and fibroscan findings in chronic hepatitis B virus infected patients.

Variables	Fibrosis score on fibroscan				
Regular edges	**Fibrosis −**	**Fibrosis +**	**Total**	**Coefficient**	**P-value**
Yes	37	30	67	11.12	0.0009
No	2	16	18		
Irregular edges					
Yes	2	16	18	13.69	0.0002
No	38	29	67		

*Fibrosis (+) = F1-F2, F3, F4; *Fibrosis (−) = F0-F1.

(a)

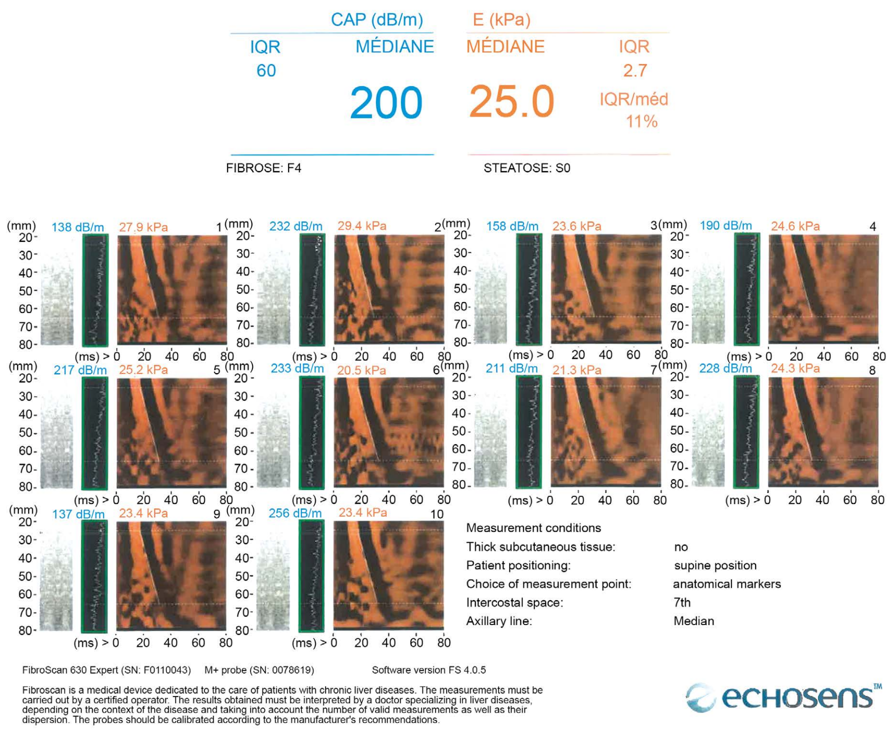

(b)

Figure 3. Cirrhosis diagnosed on ultrasound (a), correlated with severe fibrosis F4 on fibroscan (b) in a 28 years old patient followed for chronic hepatitis B virus carriage. (a): Liver with micronodular echotexture (white arrow) and irregular border (head of arrow); (b): Severe fibrosis F4 on fibroscan.

elsewhere in France, Cassinotto C. *et al.* (France 2016) found an average age of 58 years [15]. This difference could be explained by the low life expectancy of the Burkinabe population in general, which is 60 years [16] and the complications related to the natural evolution of the disease and the comorbidity factors often associated with chronic HBV infected patients in our context. In our study there was a male predominance (52.94%) with a sex ratio of 1.12. Male predominance is the most reported in the literature [1] [10] [14]. Male sex is recognized as a factor in the progression of liver fibrosis, which could partly explain their greater demand for ultrasound monitoring of the evolution of fibrosis. Furthermore, in Burkina Faso it is recognized that the majority of health expenses are supported by men [16] and therefore this could explain why they have more access to paid paraclinical examinations. The schooling rate in our study was 84.28%, other authors found figures close to ours [13] [17] [18]. This high rate of schooling in our population can be explained by the fact that the study took place in the city, where the schooling rate is generally high, but also by a better awareness of the risks among educated and informed patients. 85.88% of our study population lived in urban areas. Chronic HBV infected patients living in urban areas have better access to qualified personnel and technical facilities for their follow-up [13] [19]. All our patients were followed by a gastroenterologist who prescribed both ultrasound and fibroscan. This could be explained by the fact that good practice recommends that follow-up be done by specialists. However, given the high prevalence of HBV infection (9.1%) in the general population [20] in our country and the insufficient number of specialists, it is essential to scale up the care of patients to include general practitioners. Even though the majority of our study population was salaried or had an income-generating activity (80%), it was not possible for all patients to have both ultrasound and fibroscan. This could be explained by the fact that the expenses were supported by the patients and that the fibroscan remains a relatively expensive examination (47.54$) compared to ultrasound (15.85$) in a context where the minimum wage is 49$ in 2022.

The factors influencing the evolution of fibrosis are numerous and often associated in the same patient. In our study, only alcohol consumption was evaluated as a cofactor and 24.7% stated that they were alcohol consumers, which is a frequent phenomenon found in locoregional studies [3] [10] [13] [17] [21]. In our population 45.88% had minimal or non-significant fibrosis, 54.12% had significant fibrosis. The results are variable in the literature depending on the cohorts Diallo I *et al.* (Senegal 2016) found 57.14% of non-significant fibrosis and 42.86% of significant fibrosis [22] while Touré Ps *et al.* (Senegal 2016) found 89.9% of non-significant fibrosis, 10.1% of significant fibrosis [10].

In our study, a non-significant correlation ($p = 0.3906$) for a micronodular structure was found and this could be explained by the small sample size. Further studies with larger sample sizes are still relevant to clarify the issue. Ultrasound assessment of liver edge is a criterion associated with the diagnosis of fibrosis with the irregular type strongly associated with the diagnosis of fibrosis on fibroscan. These results are in agreement with those found in the literature, Teyssier Y *et al*. (France 2020) found a match between liver edge on ultrasound and fibrosis on fibroscan [23]. The diagnosis of steatosis, cirrhosis and dysmorphia were significantly associated with the presence of fibrosis, while hepatomegaly was not significantly associated with fibrosis. This highlights the non-significant criterion of hepatomegaly which can express several pathologies. There is a significant association between steatosis diagnosed on ultrasound and fibrosis on fibroscan. Ultrasound allows the diagnosis of steatosis with a sensitivity of over 90%. However, the hyperechogenicity of the liver parenchyma may be the expression of a fibrosis that has not progressed very far, and ultrasound cannot make the distinction at this stage [24]. These different tests between ultrasound and fibroscan show us that there is a concordance between the diagnosis of fibrosis on ultrasound and the diagnosis of fibrosis on fibroscan. These results support the use of ultrasound in the periodic follow-up of chronic HBV carriers. It should be noted that hepatic ultrasound is an indispensable means of monitoring, available, accessible, affordable, non-invasive, reliable and adapted to our context, and that access to fibroscan is limited, costly, and not available in the majority of health centres in our settings. These two examinations are complementary and cannot be dissociated in the follow-up of chronic HBV infected patients. For this reason, the new fibroscan devices are coupled with ultrasound and we speak of echo-elastometry. Certain signs should be specified in all ultrasound reports because they may indicate liver fibrosis and guide the management of chronic HBV patients. These are: hyperechoic echotexture of the liver, irregular liver edges, hepatic dysmorphia, granular appearance, hepatic steatosis, cirrhosis (but prior to the diagnosis of cirrhosis, the above signs may point to appropriate management). As our study was carried out without funding, it was subject to limitations and constraints, including the failure to carry out the fibroscan due to a lack of financial resources, the sometimes long delay between the two examinations, incomplete data in the ultrasound reports, and the non-standardization of the data, which required additional data collection via mobile phone. However, we can also consider that these results reflect real life and current practice.

5. Conclusion

Detecting the presence of fibrosis and monitoring its evolution improve the management of patients with chronic liver disease. Our study shows that ultrasound and fibroscan are complementary in the monitoring of chronic HBV infected patients. Ultrasound is a good means of monitoring due to its low cost, reliability, availability and accessibility with precise signs to look for and record in the ultrasound report. Fibroscan becomes totally relevant for those cases of fibrosis not found on ultrasound but detected as early fibrosis on fibroscan.

Conflicts of Interest

The authors declare no conflicts of interest regarding the publication of this paper.

References

[1] Diallo, S., Bassène, M.L., Gueye, M.N., *et al.* (2018) Hépatite virale B: Aspects cliniques, paracliniques et évolutifs dans le service d'Hépato Gastroentérologie de l'Hôpital Aristide Le Dantec: A propos de 728 cas. *The Pan African Medical Journal*, **31**, Article 82. https://doi.org/10.11604/pamj.2018.31.82.14725

[2] Pol, S. (2006) Histoire naturelle de l'infection par le virus de l'hépatite B. *La Presse Médicale*, **35**, 308-316. https://doi.org/10.1016/S0755-4982(06)74576-6

[3] Ntagirabiri, R., Munezero, B., Kaze, H., *et al.* (2015) Incidence du carcinome hépatocellulaire lors de l'infection chronique par le virus de l'hépatite B. *The Pan African Medical Journal*, **20**, Article 167. https://doi.org/10.11604/pamj.2015.20.167.6227

[4] World Health Organization; Geneva (2021) Hepatitis B. WHO. https://www.who.int/news-room/fact-sheets/detail/hepatitis-b

[5] Nogoma, Z. (2021) Treatment of chronic hepatitis B with nucleotide analogues in cirrhotic patients at the Centre Hospitalier Universitaire Yalgado Ouedraogo de Ouagadougou: About 38 Cases. Annale de l'université joseph Ki-Zerbo—Série D, Vol. 027.

[6] Bureau, C., Greff, M., Barthet, M., *et al.* (2010) Évaluer la fibrose: Pourquoi? Comment? Pour qui? In: Greff, M., *et al.*, Eds., *Post'U FMC-HGE*, Springer, Paris, 245-257. https://doi.org/10.1007/978-2-8178-0097-4_35 https://www.fmcgastro.org/postu-main/archives/postu-2010-paris/evaluer-la-fibrose-pourquoi-comment-pour-qui-2/

[7] Palau, R., Fortes-Déguénonvo, D. and Cadranel, J.-F. (2000) Practices of Liver Biopsy in France: Results of a Prospective Nationwide Survey. *Hepatology*, **32**, 477-481. https://doi.org/10.1053/jhep.2000.16602

[8] Bonnard, P., Sombié, R., Lescure, F.X., *et al.* (2008) M-06 Évaluation de la fibrose hépatique (histologie, marqueurs sériques, élastométrie) chez des patients infectés par le VHB au Burkina Faso. *Médecine et Maladies Infectieuses*, **38**, S168. https://doi.org/10.1016/S0399-077X(08)73179-2

[9] Bourlière, M. (2005) Comment évaluer la fibrose hépatique en dehors de la PBH. https://www.fmcgastro.org/postu-main/archives/postu-2005-paris/comment-evaluer-la-fibrose-hepatique-en-dehors-de-la-pbh/

[10] Touré, P.S., Diop, M.M., Lô, G., *et al.* (2016) Intêret du FibroScan® et des marqueurs biologiques de la fibrose hépatique, chez des sénégalais porteurs chroniques du virus de l'hépatite B faiblement réplicatifs. *Journal Africain d'Hépato-Gastroentérologie*, **10**, 14-20. https://doi.org/10.1007/s12157-015-0634-4

[11] Denis, I. (2009) Évaluation de la fibrose hépatique par l'étude de la régularité de la surface du foie en échographie haute résolution: Intérêt d'un logiciel d'analyse quantitative par rapport à une interprétation radiologique subjective. Université Joseph Fourier, Alpes.

[12] Restellini, S. and Spahr, L. (2012) Les tests non invasifs de fibrose vont-ils remplacer la biopsie hépatique? *Revue Médicale Suisse*, **2**, 1411-1415.

[13] Ouédraogo, I. (2021) Échographie de surveillance chez les porteurs chroniques l'hépatite virale b à propos de 1000 patients à ouagadougou. Ph.D. Thesis, Université Joseph Ki-Zerbo, Ouagadougou.

[14] Sombié, R., Bougouma, A., Diallo, O., *et al.* (2010) Hépatite B chronique: Aspects épidémiologique, diagnostique, thérapeutique et évolutif au centre hospitalier universitaire Yalgado Ouédraogo de Ouagadougou. *Journal Africain d'Hépato-Gastroen-*

térologie, **4**, 3-10. https://doi.org/10.1007/s12157-009-0137-2

[15] Cassinotto, C. (2016) Diagnostic et évaluation de la gravité des maladies chroniques du foie: Impact de l'elastographie par ondes de cisaillement supersonic shear imaging. Ph.D. Thèse, Université de Bordeaux, Bordeaux.

[16] INSD (2010) Enquête Démographique et de Santé Et À Indicateurs Multiples (Edsbf-Mics Iv). National Institute of Statistics and Demography (INSD), Ouagadougou. https://dhsprogram.com/pubs/pdf/pr9/pr9.pdf

[17] Diop, M., Diouf, A., Seck, S.M., *et al*. (2017) Prévalence de l'antigène de surface du virus de l'hépatite B et facteurs associés chez des militaires sénégalais envoyés en mission au Darfour. *The Pan African Medical Journal*, **26**, Article 154. https://doi.org/10.11604/pamj.2017.26.154.11594

[18] Ousmane, A., Alhousseyni, M., Laouali, H., Yahaya, I., Ousseini, A., Amadou, O., Issa, M., Zékiba, T., Lo, G. and Mounkaila, B. (2018) Facteurs de Risque et Prévalence de l'Antigène HBs chez les Femmes Enceintes et leurs Nouveau-Nés à Niamey au Niger. *Health Sciences and Disease*, **19**, 27-31.

[19] Ouavene, J.O., Koffi, B., Mobima, T., Bekondji, C., Massengue, A. and Guenebem, A.K. (2014) Cirrhoses du foie à l'hôpital de l'amitié de Bangui aspects épidémiologiques, cliniques, échographiques et problèmes de diagnostic. *Journal African d'Imagerie Médicale*, **5**, 1-12.

[20] Meda, N., Tuaillon, E., Kania, D., Tiendrebeogo, A., Pisoni, A., Zida, S., *et al*. (2018) Hepatitis B and C Virus Seroprevalence, Burkina Faso: A Cross-Sectional Study. *The Bulletin of the World Health Organization*, **96**, 750-759. https://doi.org/10.2471/BLT.18.208603

[21] Somé, E.N., Guingané, N.A., Lompo, T.I. and Sombié, R. (2021) Cirrhose du foie: Aspects épidémiologiques et diagnostiques au centre hospitalier universitaire Yalgado Ouédraogo. *Revue Africaine Des Sciences Sociales Et De La Santé Publique*, **3**, 53-64.

[22] Diallo, I., MBaye, P.S., Vray, M., *et al*. (2016) Évaluation de la fibrose dans les hépatites chroniques virales B: Comparaison entre la biopsie hépatique et l'élastométrie (Fibroscan®). *Journal Africain d'Hépato-Gastroentérologie*, **10**, 132-137. https://doi.org/10.1007/s12157-016-0663-7

[23] Teyssier, Y. (2019) Intérêt de la réduction de dimension pour évaluation de la fibrose hépatique en échographie: Approche radiomique basée sur les contours du foie. Université Grenolde d'Aples, Saint-Martin-d'Hères.

[24] Vilgrain, V. and Regent, D. (2010) Imagerie de l'abdomen La Radiologie pour tous. 1021.